frontiers in Earth Science

ORIGINAL RESEARCH
published: 10 January 2022
doi: 10.3389/feart.2021.750436

Two-End-Member Mixing in the Fluids Emitted From Mud Volcano Lei-Gong-Huo, Eastern Taiwan: Evidence From Sr Isotopes

Hung-Chun Chao[1,2], Chen-Feng You[3,4], In-Tian Lin[5], Hou-Chun Liu[3], Ling-Ho Chung[6], Chun-Chang Huang[1] and Chuan-Hsiung Chung[3,4]*

[1]Department of Earth and Environmental Sciences, National Chung Cheng University, Chiayi, Taiwan, [2]Environment and Disaster Monitoring Center, National Chung Cheng University, Chiayi, Taiwan, [3]Department of Earth Sciences, National Cheng Kung University, Tainan, Taiwan, [4]Earth Dynamic System Research Center, National Cheng Kung University, Tainan, Taiwan, [5]Exploration and Development Research Institute, CPC Corporation, Miao-li, Taiwan, [6]National Museum of Natural Science, Taichung, Taiwan

OPEN ACCESS

Edited by:
Guodong Zheng, Northwest Institute of Eco-Environment and Resources (CAS), China

Reviewed by:
Galip Yuce, Hacettepe University, Turkey
Giovanni Martinelli, National Institute of Geophysics and Volcanology, Italy

***Correspondence:**
Hung-Chun Chao
hcchao@ccu.edu.tw
ekman60@gmail.com

Specialty section:
This article was submitted to Geochemistry, a section of the journal Frontiers in Earth Science

Received: *30 July 2021*
Accepted: *30 November 2021*
Published: *10 January 2022*

Citation:
Chao H-C, You C-F, Lin I-T, Liu H-C, Chung L-H, Huang C-C and Chung C-H (2022) Two-End-Member Mixing in the Fluids Emitted From Mud Volcano Lei-Gong-Huo, Eastern Taiwan: Evidence From Sr Isotopes. Front. Earth Sci. 9:750436. doi: 10.3389/feart.2021.750436

Mud volcano is one of the most important conduits for deep seated materials to migrate upward in sedimentary basins, convergent margins, and subduction zones. Understanding their temporal and spatial characteristics and variations provides us the important information on fluid sources and chemical compositions at depth. Mud volcano Lei-Gong-Huo (MV LGH) is a unique mud volcano, which is located on the mélange formation lying on the andesitic volcanic arc. Fluids emitted from 46 mud pools in MV LGH in eastern Taiwan were sampled and their major trace constitutes as well as H, O, and Sr isotopes ($^{87}Sr/^{86}Sr$ and $\delta^{88}Sr$) were measured. Major constitutes of the fluids are Cl^-, Na, and Ca. Compared with seawater, LGH fluids have lower Cl^-, δD, $\delta^{18}O$, Na/Cl, K/Cl, and Mg/Cl but higher Ca/Cl ratios, indicating water–rock interaction of igneous rock and the ancient seawater at the source region. This interpretation is further supported by Sr isotopes, which show low value of $^{87}Sr/^{86}Sr$ ratio down to 0.70708. The result of spatial distribution showing strong negative correlation between Na and Ca concentration as well as Ca and $^{87}Sr/^{86}Sr$ ratios indicates that two end-member mixing is the major chemical characteristic. The fluids interacting with igneous rock carry high Ca, high $\delta^{88}Sr$, low Na, and low $^{87}Sr/^{86}Sr$ ratio, while those interacting with sedimentary rock carry low Ca, low $\delta^{88}Sr$, high Na, and high $^{87}Sr/^{86}Sr$ ratio. The source from the igneous region dominates the eastern and southeastern parts of the mud pools while sedimentary source dominates the western and northwestern parts. Most mud pools show mixing behavior between the two sources. Some of the sedimentary-dominated mud pools reveal existence of residual ancient water as indicated by $^{87}Sr/^{86}Sr$. The major factor to fractionate the stable Sr isotopes in LGH waters is the source lithology. In summary, fluids emitted by mud pools in LGH originate from two sources, which are water–rock interactions of igneous rock with the ancient seawater from the east and sedimentary rock from the west at depth, resulting from the complex geologic background of mélange formation.

Keywords: mud volcano, radiogenic Sr isotopes, stable Sr isotopes, sediment-hosted geothermal systems, water–rock interaction

INTRODUCTION

Mud volcanoes (MVs) are one of the most efficient structures for the fluids at depth to migrate through thick sediments to the surface. They are a common diapiric feature in convergent margins where soft, thick, and fine-grained mud is rapidly deposited and sediment porosity is reduced by tectonic compaction. With the hydrocarbon gases production and generation at depth, the buoyancy of the fluid is enhanced and the strength of the formation is weakened. The development of the mud diapir or the fault provides the pathway for the fluid to migrate upward (Milkov, 2000; Dimitrov, 2002; Kopf, 2002; Mazzini and Etiope 2017). Terrestrial MVs are documented worldwide such as those in Italy, Azerbaijan, Romania, Taman (Russia), Georgia, Iran, Pakistan, Andaman (India), Indonesia, Taiwan, Japan, Sakhalin (Russia), Trinidad, and so on (Dia et al., 1999; Delisle et al., 2002; Etiope et al., 2002; Planke et al., 2003; Shakirov et al., 2004; Yang et al., 2004; You et al., 2004; Lavrushin et al., 2005; Mazzini et al., 2007; Deville and Guerlais 2009; Mazzini et al., 2009; Etiope et al., 2011a; Etiope et al., 2011b; Ray et al., 2013; Lavrushin et al., 2015; Omrani and Raghimi, 2018; Farhadian Babadi et al., 2019; Farhadian Babadi et al., 2021), and there are probably 10 times more submarine MVs than terrestrial ones (Milkov, 2000; Mazzini and Etiope 2017).

The substances emitted by MVs exist in gas, liquid, and solid phases. The gases are mainly composed of methane (>90%) with minor amounts of nitrogen, argon, carbon dioxide, ethane, and higher hydrocarbon gases (Etiope et al., 2002; Shakirov et al., 2004; Yang et al., 2004; Etiope et al., 2007; Etiope et al., 2009; Chao et al., 2010; Sun et al., 2010). Some MV gases are dominated by CO_2 (Etiope et al., 2002; Shakirov et al., 2004; Yang et al., 2004; Chao et al., 2010), probably associated with the sediment-hosted geothermal system (Procesi et al., 2019). Globally, more than 76% of MVs expel thermogenic gases, only 4% of MVs expel microbial hydrocarbon gases, and the rest expel mixed gases (Etiope et al., 2009). In general, the liquid phase (water) of mud volcano fluids originates from marine sedimentary pore fluids. The water may have experienced important diagenesis and/or have been influenced by clay dehydration, water–rock interaction, halide dissolution, and may mix with groundwater, surface runoff, and meteoric water near the land surface (Bray and Karig, 1985; Dia et al., 1999; Dählmann and de Lange, 2003; You et al., 2004; Mazzini et al., 2009). The solid matter is mainly derived from the ambient sediments surrounding the fluid reservoirs or the migration channel, mostly clay minerals, such as smectite, illite, kaolinite, chlorite, quartz, and calcite (Shih, 1967; Dia et al., 1999; Kopf and Deyhle, 2002; Farhadian Babadi et al., 2019). The origination of all three phases may decouple from each other (Sun et al., 2010; Mazzini et al., 2018).

Strontium (Sr) has four naturally occurring stable isotopes, ^{84}Sr, ^{86}Sr, ^{87}Sr, and ^{88}Sr, where ^{87}Sr is a radiogenic product of ^{87}Rb through beta decay with a half-life of 48.8 Ga (Banner, 2004). Since the variations of radiogenic Sr isotope ($^{87}Sr/^{86}Sr$) are controlled by the age and the Rb/Sr ratio of the source materials and it is a general consensus that $^{87}Sr/^{86}Sr$ will not be fractionated by biological and low-temperature abiotic chemical reactions, $^{87}Sr/^{86}Sr$ has become a powerful tool for provenance identification in hydrology (Palmer and Edmond, 1992; Douglas et al., 2003; Liu et al., 2011), archaeology (Alexander Bentley, 2006), and food authentication (Fortunato et al., 2004), as well as the fluid source of MVs (Dia et al., 1995; Chao et al., 2013; Mazzini et al., 2018; Bujakaite et al., 2019). On the other hand, fractionation of stable Sr isotope ($^{88}Sr/^{86}Sr$) in the hydrosphere provides complement information such as incongruent weathering (Wei et al., 2013; Chao et al., 2015), carbonate precipitation (Chao et al., 2013; Fruchter et al., 2017; Liu et al., 2017; Shao et al., 2021), carbonate recrystallization (Voigt et al., 2015), and degree of water–rock interaction (Krabbenhöft et al., 2010; Voigt et al., 2018).

Fluids expelled by the eastern Taiwan MVs have different chemical characteristics from those expelled by the western ones. Their major elements show signature of rock–rock interaction with igneous rocks with $^{87}Sr/^{86}Sr$ lower than 0.708 (You et al., 2004; Chao et al., 2013). The geological sedimentary structure emits water containing geothermal signal. This hybrid characteristic matches the sediment-hosted geothermal system (Procesi et al., 2019). Large $^{87}Sr/^{86}Sr$ variation in different mud pools are also reported (Chao et al., 2013), implying the possibility of multiple sources. In this study, fluids from two eastern Taiwan MVs were sampled monthly in 10 campaigns. The major and trace ions/elements, hydrogen, oxygen, and strontium isotopic compositions of the water samples separated from the fluids were measured. The systematic measurements with the time–series investigations help to decipher the origin(s) of the fluids and clarify the hybrid system.

MATERIALS AND METHODS

Geological background and site description

Taiwan is located at the plate boundary between the Philippine Sea Plate and the Eurasian Plate, where the Taiwan mountain belt was formed as a result of arc–continent collision (Li, 1976; Teng, 1990). The Luzon Arc moves northeast toward the Asian continent at an average rate of 7 cm per year (Yu et al., 1997). Across the Longitudinal Valley Fault (LVF), the fast speed of the movement decreases dramatically from the arc (Coastal Range) of 7 cm per year to the continent (Central Range) of 2 cm per year (Ching et al., 2011). The highly deformed Lichi Mélange formation, which was the forearc basin and composed of chaotic mudstone intermixed with exotic blocks of various sizes and lithology including fragments of oceanic crust (Chang et al., 2000), may be the substance that absorbs the movement of 5 cm per year (Ching et al., 2011) and provides the suitable environment for the formation of MVs.

Two MVs are located on the hanging wall of the Lichi Fault in the Lichi Mélange and the foothill of the Coastal Range (**Figures 1A, B**). In the south, MV Lei-Gong-Huo (LGH) appears as an elongated mud shield with an area about 150 m long and 50 m wide (**Figures 1C–E**). On the top of the mud shield, dozens of mud pools from about 10 cm to 2 m in diameter are distributed along the direction of approximately N15°W (NNW–SSE). The mud pools in the south are distributed linearly, but the northern ones are sparsely distributed (**Figure 1C**). A total of 46 mud pools

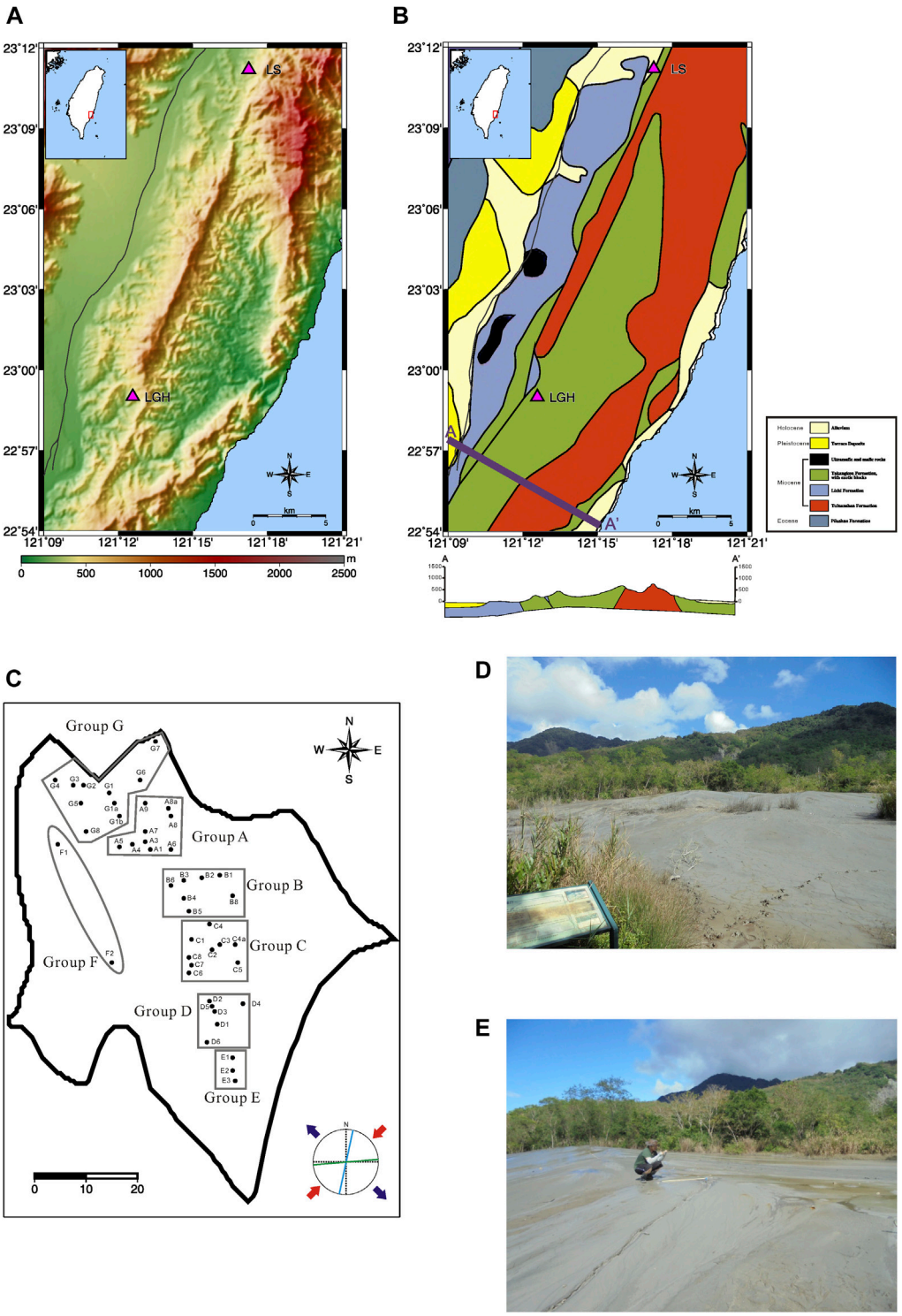

FIGURE 1 | (A) Mud volcano sampling sites (triangles), **(B)** geologic map adopted from Lin et al. (2008) as well as schematic cross section of A—A′ profile shows forearc basin, active thrust fault, and andesitic volcanic arc. **(C)** Mud-covered area of MV LGH (solid line) and the location of each sampled mud pool (black dots). Local fracture analysis in Stereonet after the 2003 M_w = 6.8 earthquake by Jiang et al. (2011) is shown for reference. **(D)** Photograph of MV LGH view from the entrance (the westernmost spot) to groups B and C. **(E)** Photograph taken on the axis of the mud shield, view from group E to group B and C, heading north.

in this area were sampled from October 2015 to July 2016 monthly and more than half of them are short-lived ones. Not all mud pools were sampled except the November 2015, May 2016, and July 2016 visiting. Seven groups in the MV LGH are classified according to their locality (**Figure 1C**). Group A to E are five clusters of mud pools distributed from north to south along the axis of the mud shield, and group F is the mud pools on the western flank. Mud pools in the northwestern corner belong to group G. In the north, MV Luo-Shan (LS; previously also named Yencheng by Shih, 1967) contains dozens of linearly distributed swamp-like mud pools with larger coverage, approximately 1 km in length and 200 m in width, and have a direction of N20°E (NNE-SSW), parallel to the strike of the Lichi Mélange formation and major faults. Due to the single fluid source of MV LS (Chao et al., 2013), only the most active one, LS-A1, has been sampled as the reference site.

MVs LGH and LS emit predominantly methane (>90%), similar to typical sedimentary MVs. However, low CO_2 (<0.2%) in both MVs with higher N_2 concentration (>5%) and mantle helium signals of MV LS (Yang et al., 2003; Yang et al., 2004; Chao et al., 2010) show different gas composition compared with sedimentary MVs. MV LS emits thermogenic methane, but MV LGH emits methane of a mix of thermogenic and microbial sources (Chao et al., 2010; Sun et al., 2010). The Sr isotopes of the fluids in LS show the typical and consistent igneous characteristics for all MVs collected in this area (You et al., 2004; Chao et al., 2013) but LGH has stronger sedimentary contributions with larger $^{87}Sr/^{86}Sr$ distribution, although there are only two samples presented (Chao et al., 2013).

Sampling

MV fluid samples were collected approximately 20 cm right below the gas bubbling area using four 50-cm^3 polypropylene (PP) centrifuge tubes. The temperature, pH, and oxidation-reduction potential (ORP) values were obtained on site with a WalkLAB® TI9000 temperature compensation pH meter. After centrifuge, samples were filtered with 0.45-μm nylon membrane filters. The percentage of mud weight was determined by the weight of the mud after 50°C drying in the oven over the weight before centrifuge. For each sample, approximately 60 ml of the filtered solution was acidified with purified concentrated nitric acid to pH <2 for determination of major, trace elements, and Sr isotopes. Unacidified samples were preserved for the measurement of anion concentrations, total alkalinity, and water isotopes. All samples were kept at 4°C in the refrigerator for later analysis.

Chemical composition of the fluids

Dissolved anions (Cl^-) were determined using ion chromatography (Dionex® ICS-3000) with a precision of 5%, and quality assurance was obtained by the diluted international seawater standard IAPSO. Chloride concentration is calculated based on the salinity of IAPSO and the equation established by Millero et al. (2008). Major and trace elements (B, Ba, Ca, Fe, K, Li, Mg, Mn, Na, S, Si, and Sr) were measured using Agilent 5100 inductively coupled plasma optical emission spectrometry (ICP-OES) with a precision of better than 3%. Total alkalinity (TA) was measured with acid titration (Metrohm® 905 Titrando) with the precision better than 1%, estimated by repeating the analyses of the sample ($n = 3$) and in-house-prepared bicarbonate standard.

Water isotopes

H and O isotopes were obtained by the cavity ring-down spectroscopy (CRDS, H_2O isotope analyzer, Picarro L2140-i) installed at the Exploration and Development Research Institute, CPC Corporation, Taiwan (EDRI). Instrumental fractionation was corrected by measuring two international standards (V-SMOW2 and SLAP2). This correction was certified by a third international standard (GISP). For drift correction and quality control, four USGS standards of known δD and $\delta^{18}O$ values (USGS-45, USGS-47, USGS-48, and USGS-50) were analyzed after six consecutive samples were run. The reproducibility of δD and $\delta^{18}O$ is better than 0.1‰ and 0.03‰ (2σ, $n = 6$), respectively, by repeating the analyses of some selected samples. All δD and $\delta^{18}O$ isotopic results reported in this study were normalized to V-SMOW2.

Strontium isotopes

The separation and purification of Sr were performed using an extraction chromatography technique, Sr Spec® resin (Eichrom Technologies, USA). The procedure was modified from the published protocol by Ohno et al. (2008). In brief, 360 ng of Sr, which is enough for triple measurements, from the samples was evaporated to dryness and redissolved in 1 ml 2 M of HNO_3. Acid-cleaned PP columns with an inner diameter of 5 mm were loaded with 1 ml of Eichrom Sr Spec® resins (100–150 mesh). After 2 ml 2 M of HNO_3 precondition, most of the potential matrix and isobaric interference elements such as Ca, Na, Rb, and Zr were eliminated by the first 6 ml 2 M of HNO_3, and Ba was removed by the following 6 ml 7 M of HNO_3. The presence of Ba in the sample solution causes significant isotope fractionation of the stable Sr in the mass spectrometer (de Souza et al., 2010; Chao et al., 2013; Scher et al., 2014). At last, the Sr fraction was collected by 6 ml of deionized water, evaporated to dryness, and redissolved in 2.4 ml 0.3 M of HNO_3 in sequence. The elution curve shows the recovery of Sr is higher than 98%.

The Sr isotopic composition of fluid samples was determined using a multicollector inductively coupled plasma mass spectrometer (MC-ICP-MS, Neptune, Thermo Fisher Scientific) installed at the Earth Dynamic System Research Center, National Cheng-Kung University. A modified empirical external normalization (EEN, Liu et al., 2012) with the traditional standard-sample-bracketing (SSB) technique was used to correct instrumental mass bias. After column purification, sample solutions were adjusted to a final concentration of 150 ppb Sr with spiked 300 ppb Zr (High-Purity Standards®) in 0.3 M HNO_3. ^{86}Sr, ^{87}Sr, ^{88}Sr, ^{90}Zr. and ^{92}Zr ion-beams were collected simultaneously in a static mode. ^{85}Rb and ^{83}Kr were monitored for the correction of ^{87}Rb contribution on ^{87}Sr and ^{86}Kr on ^{86}Sr. The mass bias correction for traditional $^{87}Sr/^{86}Sr$ ratio was based on the assumption of constant $^{88}Sr/^{86}Sr$ ratio (8.375, 209). The monitored $^{92}Zr/^{90}Zr$ ratio was applied for mass bias correction on $^{88}Sr/^{86}Sr$ determinations.

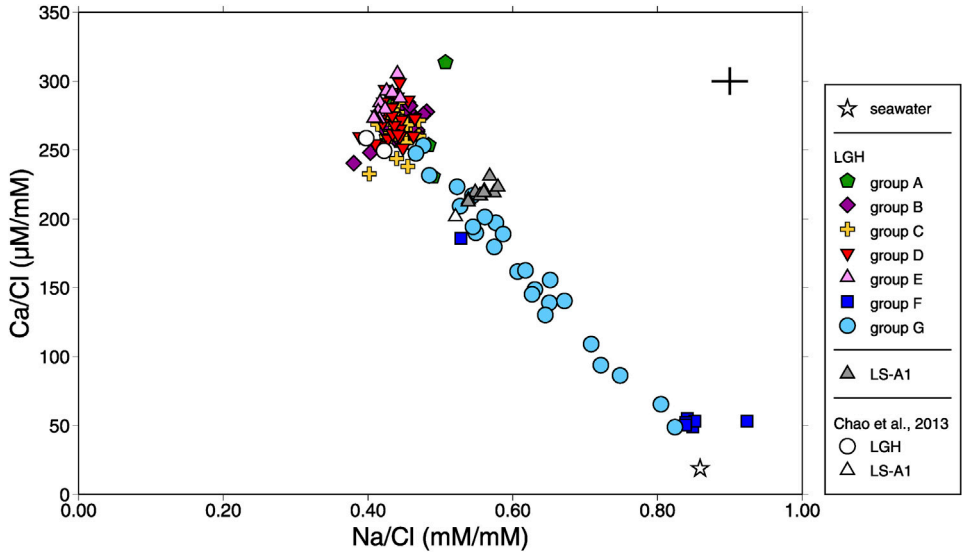

FIGURE 2 | Plot of Ca/Cl ratio vs. Na/Cl ratio for all mud volcano fluids in this study. Previous report (Chao et al., 2013) and seawater composition are shown for reference. The range of the cross denotes the range of the reproducibility (2σ).

The reproducibility of $^{87}Sr/^{86}Sr$ and $\delta^{88}Sr$ in the international seawater standard IAPSO and the inhouse seawater LMN_4-3 is better than 0.000014 and 0.026‰ (2σ, $n = 5$) with the values of 0.709, 178, 0.378‰, and 0.709, 173, 0.380‰ respectively. The $\delta^{88}Sr$ results are expressed using conventional notation modified after Krabbenhöft et al. (2009):

$$\delta^{88}Sr = \left[\frac{{}^{88}Sr/{}^{86}Sr_{sample}}{{}^{88}Sr/{}^{86}Sr_{NBS\,SRM\,987}} - 1\right] \times 10^3 \ (‰) \qquad (1)$$

where $^{88}Sr/^{86}Sr_{sample}$ and $^{88}Sr/^{86}Sr_{standard}$ denote the $^{88}Sr/^{86}Sr$ ratios in the sample and standard respectively.

RESULTS

Both MVs in this study show similar chemical and isotopic results compared with previous reports (Yeh et al., 2005; Chao et al., 2011; Chang et al., 2012; Chao et al., 2013). MV LGH has higher total dissolved solids (TDS) than MV LS and has approximately 50% and 35% TDS relative to seawater respectively. Cl, Na, and Ca are the most abundant elements in the water of MV fluids (**Supplementary Table S1**). Chloride content in the waters of LGH ranges from 186 to 376 mM with an average value of 334 mM. Sodium concentration ranges from 131 to 289 mM with an average value of 160 mM. Calcium ranges from 16 to 99 mM with an average value of 82 mM. The average Cl, Na, and Ca concentrations of MV LS-A1 are 215, 119, and 47 mM, respectively. The trace ions or elements are Mg, B, TA, K, Ba, Sr, Si, S, Mn, Li, and Fe, listed in the order of concentration.

In comparison with seawater, MV fluids in eastern Taiwan have lower Na/Cl but higher Ca/Cl ratios, showing different major element/Cl ratios pattern versus those in the western ones and possibly resulting from water–rock interaction with igneous rocks at low temperature (Chao et al., 2011; Chao et al., 2013). The results show small temporal variations in MV LS-A1 with Na/Cl ratios at 0.53 to 0.58, lower than the seawater value of 0.86, and Ca/Cl ratios at 0.21 to 0.23, two orders of magnitude higher than the seawater value of 0.018 (**Figure 2**). However, MV LGH shows large spatial variation. The Na/Cl ratios are distributed from 0.38 to 0.92 and Ca/Cl ratios are distributed from 0.049 to 0.31. Although the Cl concentration shows minor variations among seven groups, Na and Ca have strong negative correlation (r = −0.92; **Supplementary Table S2** and **Figure 3**). Low Ca with high Na fluids are distributed at the northwestern side of the MV field (i.e., groups F and G) while high Ca with low Na fluids are located at the southern side (i.e., group E; **Figure 1C**). Other trace element/Cl ratios show similar characteristics with typical terrestrial and marine sedimentary MVs characterized by lower Mg/Cl and higher B/Cl, Ba/Cl, Li/Cl, and Sr/Cl ratios relative to seawater (e. g., Dia et al., 1995; Lavrushin et al., 2003; Aloisi et al., 2004; Chao et al., 2011; Farhadian Babadi et al., 2019; Chen et al., 2020).

Sr isotopes, both stable and radiogenic, have similar characteristics to major elements. LS-A1 has relatively small temporal isotope variations, between 0.70676 and 0.70683 with a mean value of 0.70678 and between 0.29‰ and 0.34‰ with a mean value of 0.32‰ for $^{87}Sr/^{86}Sr$ and $\delta^{88}Sr$, respectively (**Figures 4** and **5**). Both radiogenic and stable Sr isotopes of MV LGH show large variations compared with LS-A1 and their values range between 0.70708 and 0.71132, and between 0.23‰ and 0.38‰, respectively (**Figures 4** and **5**). LGH has overall higher $^{87}Sr/^{86}Sr$ ratios but similar average $\delta^{88}Sr$, 0.31‰, relative to LS-A1.

Unlike Sr isotopes, δD and $\delta^{18}O$ in MV water show small variation spatially and temporally. LS-A1 water has δD distributed between −3.7‰ and -2.2‰ with a mean value of −2.7‰ and $\delta^{18}O$ varies from −0.70‰ to −0.35‰ with a mean value of −0.55‰. δD and $\delta^{18}O$ in MV LGH are distributed from

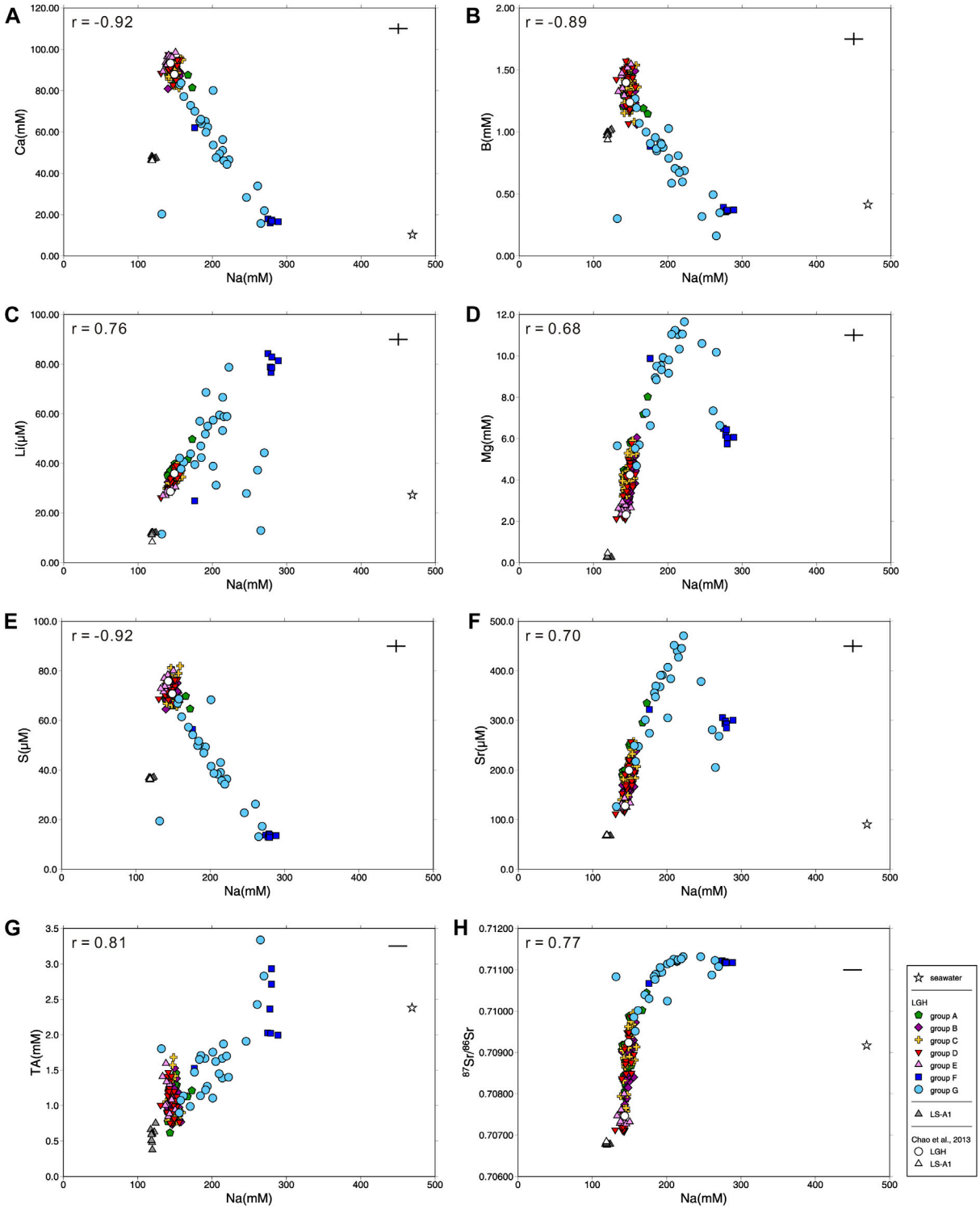

FIGURE 3 | Plot of **(A)** Ca vs. Na, **(B)** B vs. Na, **(C)** Li vs. Na, **(D)** Mg vs. Na, **(E)** S vs. Na, **(F)** Sr vs. Na, **(G)** total alkalinity vs. Na, **(H)** $^{87}Sr/^{86}Sr$ vs. Na, **(I)** B vs. Ca, **(J)** Li vs. Ca, **(K)** Mg vs. Ca, **(L)** S vs. Ca, **(M)** Sr vs. Ca, **(N)** total alkalinity vs. Ca, and **(O)** $^{87}Sr/^{86}Sr$ vs. Ca for all mud volcano fluids in this study with Pearson's correlation coefficient r and literature results (Chao et al., 2013) for comparison. Seawater composition is shown for reference and the range of the cross denotes the range of the reproducibility (2σ).

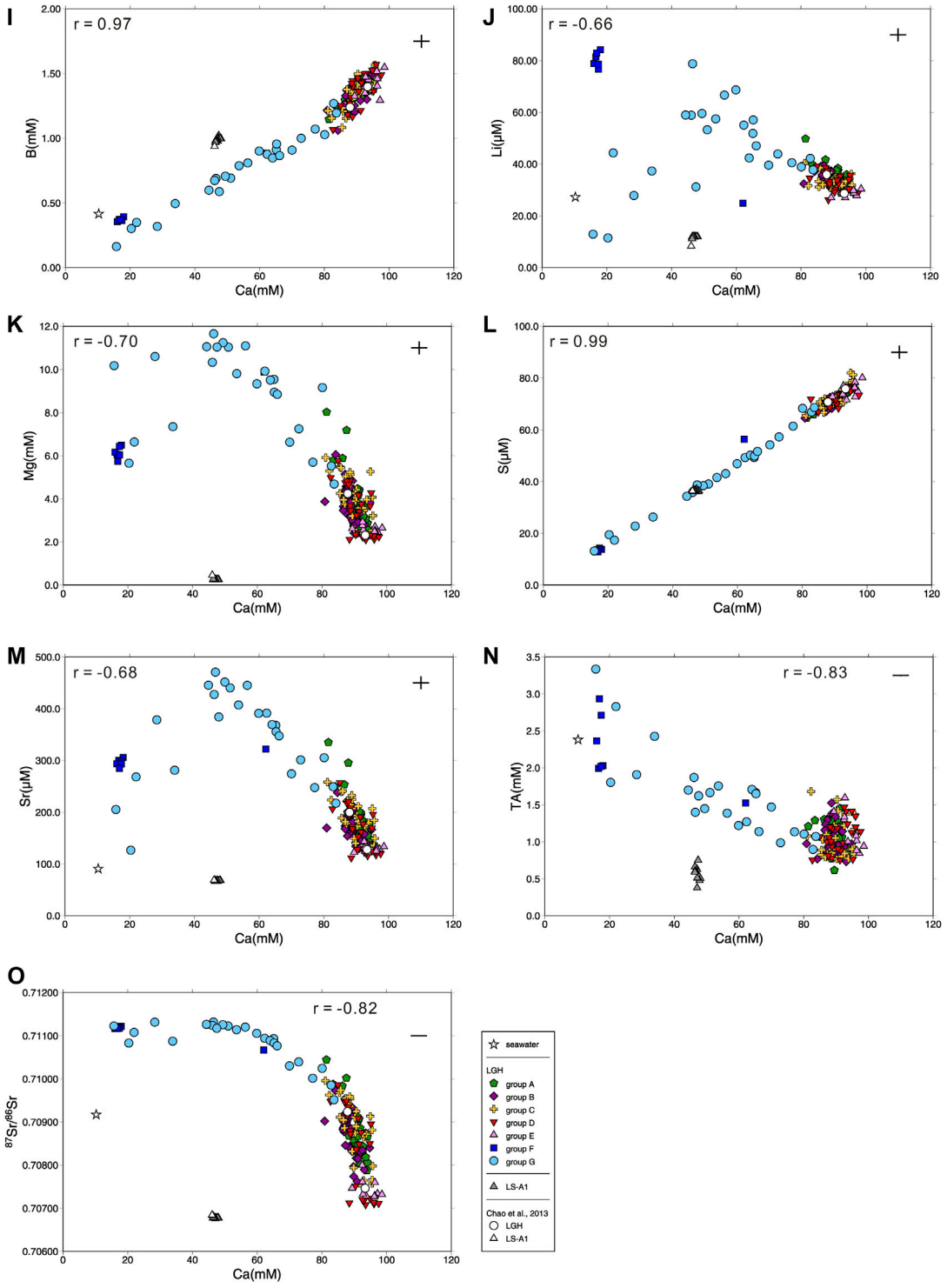

FIGURE 3 | (continue)

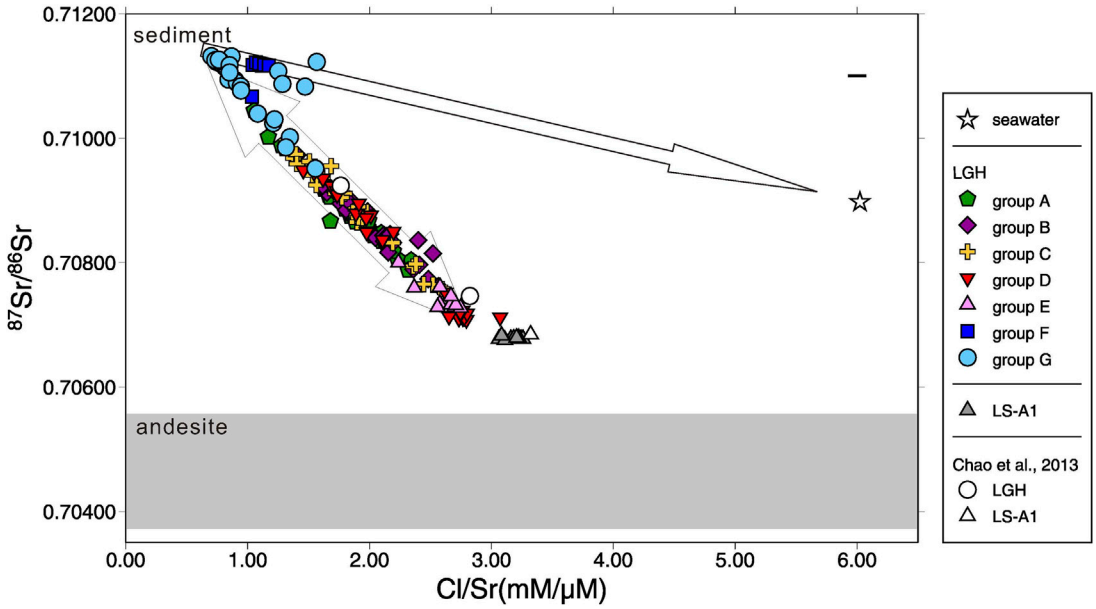

FIGURE 4 | Plot of $^{87}Sr/^{86}Sr$ vs. Cl/Sr ratio for all mud volcano fluids in this study. Seawater composition, literature results (Chao et al., 2013), and the arc basement (andesite; shaded area) are shown for reference. The range of andesite $^{87}Sr/^{86}Sr$ is adopted from Chen et al. (1990) and Bentahila et al. (2008). Variation of the ancient seawater since 5 Ma is smaller than the symbol. The range of the cross denotes the range of the reproducibility (2σ).

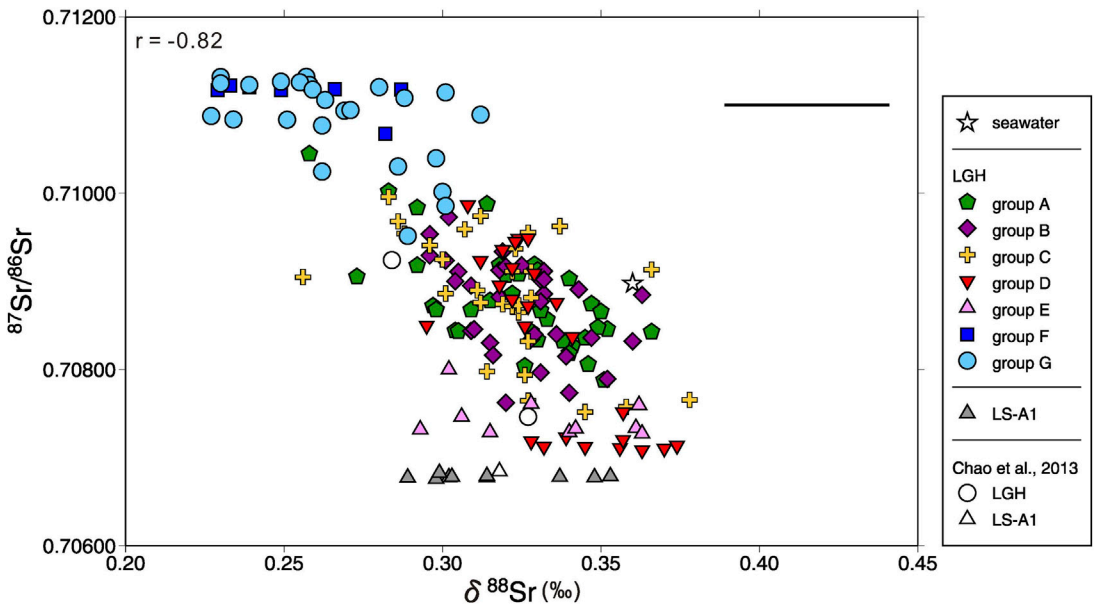

FIGURE 5 | Plot of $^{87}Sr/^{86}Sr$ vs. $\delta^{88}Sr$ for all mud volcano fluids in this study. Pearson's correlation coefficient r and seawater composition are shown for reference. The range of the cross denotes the range of the reproducibility (2σ).

−8.5‰ to 2.3‰ and −1.94‰–0.82‰ with a mean value of −3.6‰ and −1.27‰, respectively (**Figure 6**). The average values of δD and $\delta^{18}O$ in LS are slightly higher than those in LGH. The statistical results of Student's t-test indicate distinguishable isotopic composition between the two MVs ($p < 0.001$ for both water isotopes). Considering the groups in LGH, group E of LGH has indistinguishable water isotopes with LS-A1 ($p > 0.9$ and >0.6 for δD and $\delta^{18}O$, respectively). Groups E and F show distinguishable δD and $\delta^{18}O$ distribution, but other groups reveal no distinctive water isotope characteristic (**Figure 6**).

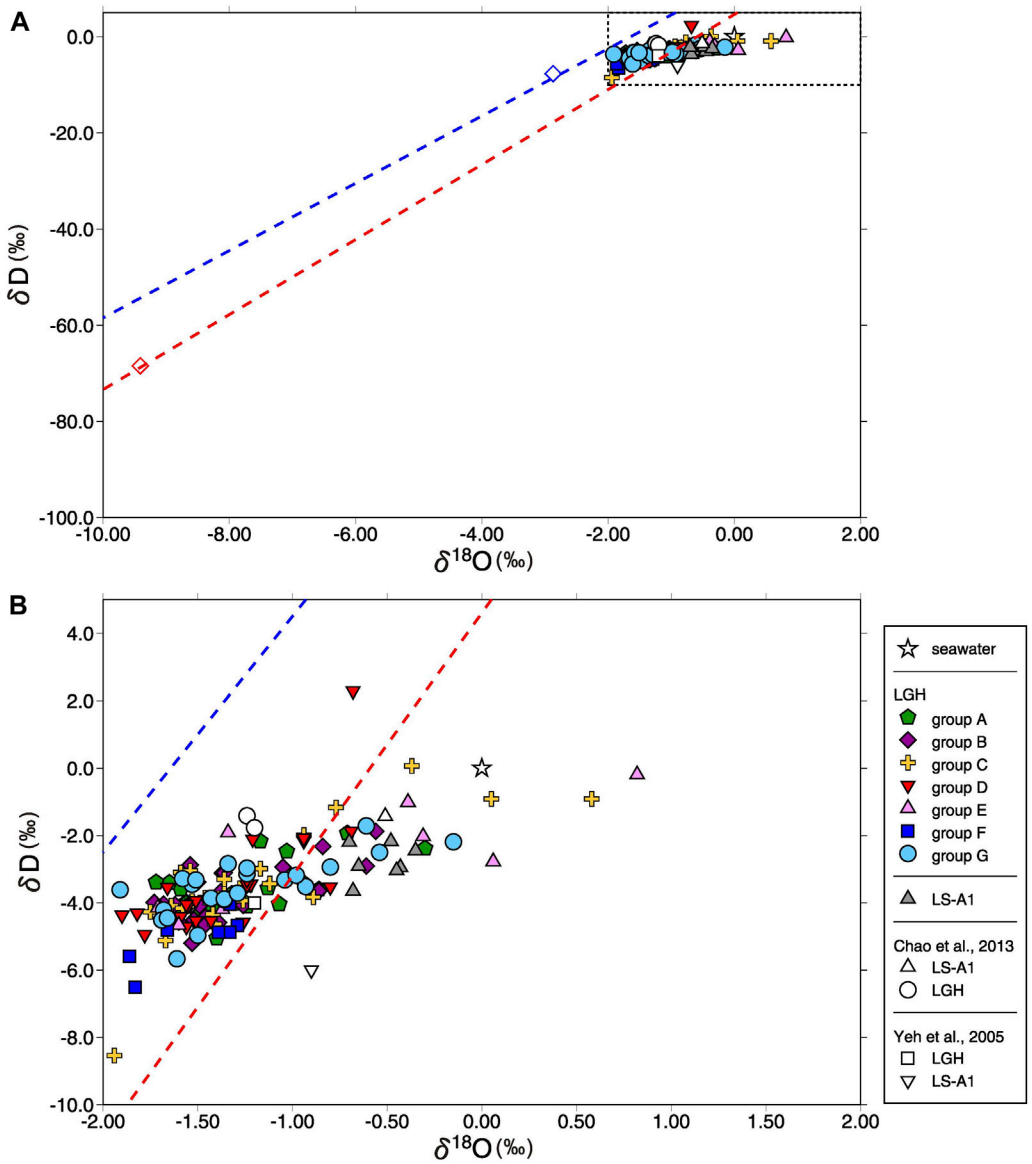

FIGURE 6 | Plot of δD vs. $\delta^{18}O$ for **(A)** all mud volcano fluids in this study, **(B)** zoom out of the dashed area. Seawater composition, literature results (Yeh et al., 2005; Chao et al., 2013), and local meteoric water line (Peng et al., 2010) are shown for reference. Blue dash line denotes local meteoric water line of the winter monsoon with the volume weighted average value (open blue diamond) and red dash line denotes local meteoric water line of the summer monsoon with the volume weighted average value (open red diamond). The reproducibility is smaller than the symbol. The slope of increasing trend is approximately 2, possibly implying local evaporation line.

However, by excluding the low d-excess samples, which possibly resulted from evaporation, groups E and F display no statistical differences. The overall O and H isotopes in LGH MV water denote a positive correlation with the slope of approximately 2, possibly indicating local evaporation line.

DISCUSSION

MV fluids closed to marine environments denote similar chemical characteristics to deep marine pore fluids which originate from ancient seawater and have been altered by early diagenesis, clay dehydration, and water–rock interaction (e.g., Dia et al., 1999; Dählmann and de Lange, 2003; Hensen et al., 2004; You et al., 2004; Mazzini et al., 2007; Mazzini et al., 2009; Ray et al., 2013; Farhadian Babadi et al., 2019; Chen et al., 2020). These mechanisms result in the dissolved constituents of MV fluids generally showing lower chloride concentration, lower Mg/Cl, Ca/Cl, and δD ratios with higher Na/Cl, B/Cl, Li/Cl, Ba/Cl, Br/Cl, I/Cl, and $\delta^{18}O$ ratios compared with seawater (e.g., Dia et al., 1995; Lavrushin et al., 2003; Aloisi et al., 2004; Chao et al., 2011; Farhadian Babadi et al., 2019; Chen et al., 2020). Although chemical and isotopic compositions of MV fluids in LS and LGH match most of the features, they present reverse relationship between Na/Cl and Ca/Cl

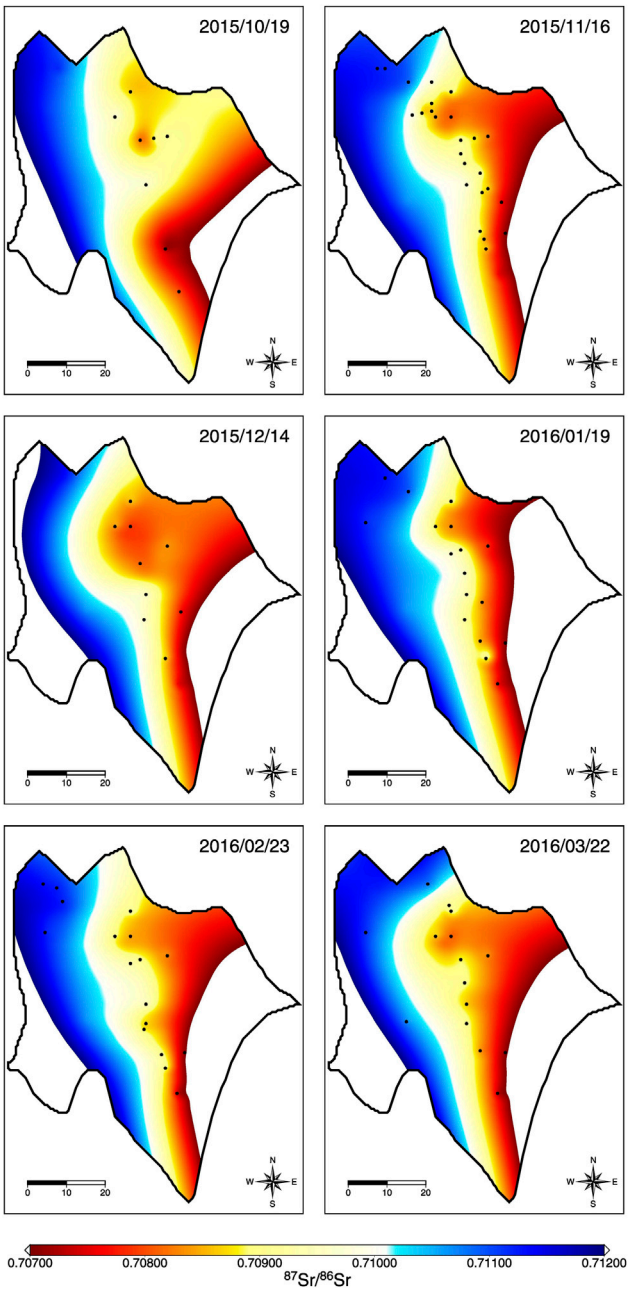

FIGURE 7 | The colored contour distribution of $^{87}Sr/^{86}Sr$ for MV LGH on 10 campaigns. Black dots denote sampled mud pools. The full sampling of the mud pools was achieved on November 2015, May 2016, and July 2016. Plenty of mud pools were buried by mud flow induced by heavy rainfall before the campaign on July 2016. The unit of scale bar is meter. Low $^{87}Sr/^{86}Sr$ end member dominates eastern and southeastern side of the field while high $^{87}Sr/^{86}Sr$ end member dominates western and northwestern side. Southeastern side shows consistent situation during the sampling period while northwestern side and the central part display variations.

ratios compared with typical sedimentary MVs. Laboratory hydrothermal experiments at temperature lower than 80°C (Seyfried and Bischoff, 1979; Henderson, 1982) and evidence from marine pore water (e.g., Gieskes et al., 1975; Perry et al., 1976; Lawrence and Gieskes, 1981; Gieskes et al., 1990) indicate this chemical characteristic is caused by low temperature water–rock interaction with volcanic ash and/or igneous rock. The $^{87}Sr/^{86}Sr$ ratio of the fluids further supports this observation (**Supplementary Table S1**; **Figure 4**). MV fluids in eastern Taiwan show strong geochemical characteristic of water–rock interaction with igneous rock. However, the covariation of Na, Ca, Mg, B, Ba, Sr, S, Li, total alkalinity, as well as $^{87}Sr/^{86}Sr$ and $\delta^{88}Sr$ may indicate a two-end-member-mixing system dominates the geochemical characteristic of MV LGH.

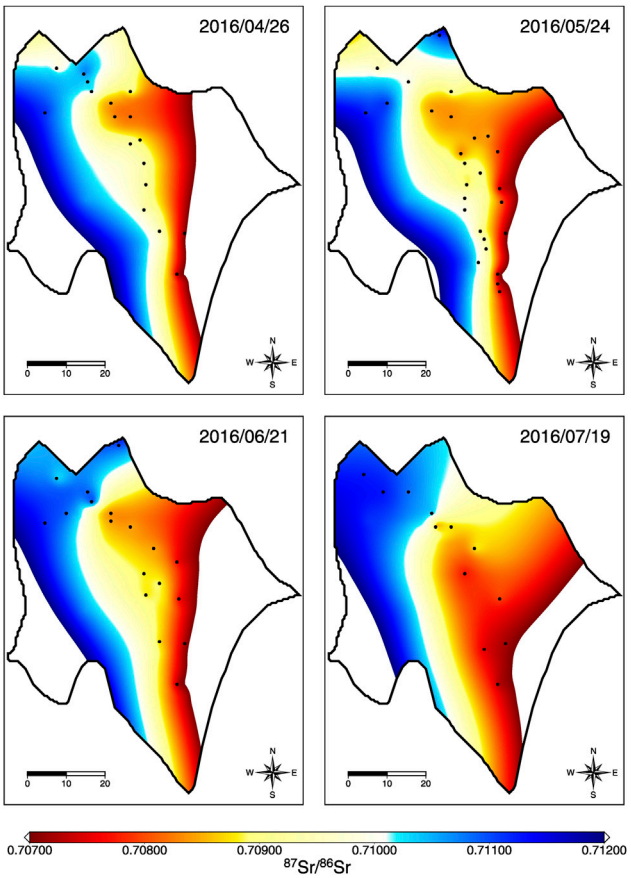

FIGURE 7 | (continue)

Chemical and isotope distribution of the fluids in mud volcano Lei-Gong-Huo

Radiogenic Sr isotope, $^{87}Sr/^{86}Sr$, is a robust tool to decipher the source of the fluids. The fluids involved with sedimentary and igneous rocks are the best objects because of the distinct end members. By comparing the correlation between the chemical composition and $^{87}Sr/^{86}Sr$ ratio of the fluids in LGH, two major end members are revealed. One is the fluid interacted with sediments, which are possibly inside the Lichi Mélange. The other is the fluid interacted with igneous rocks, which are the andesitic volcanic arc in the east also the basement of the Coastal Range (**Figure 1**). Sedimentary fluid carrying $^{87}Sr/^{86}Sr$ ratio higher than seawater, high Na, Mg, Sr, and Ba concentrations, and low Ca, S, and B concentrations with low $\delta^{88}Sr$ is distributed in the northwestern area while andesitic fluid carrying low $^{87}Sr/^{86}Sr$ ratio, low Na, Mg, Sr, and Ba concentrations, and high Ca, S, and B concentrations with higher $\delta^{88}Sr$ is located at the southeastern side (**Figures 3** and **7**; **Supplementary Table S1**). LGH-D4 and group E are the representatives of andesitic fluids, while groups F and G can be the representatives of sedimentary fluids (**Figures 3** and **7**). The other groups located on the axis of the mud shield emit fluids mixing with two end members (**Figures 3** and **7**). However, some sedimentary-fluid-dominated mud pools (i.e., LGH-F1, LGH-G5, LGH-G6, and LGH-G8) do not fall on the mixing line between the two major end members and a trend toward ancient seawater can be extrapolated (**Figure 4**), indicating contribution of residual seawater to a sedimentary end member.

Chao et al. (2013) reported large $^{87}Sr/^{86}Sr$ variations by two MV fluids collected in LGH in the year 2008. This chemical characteristic of two-end-member-mixing has lasted at least since the year 2008. The mud pools distributed on the axis of the mud shield (e.g., LGH-A1, LGH-B1, LGH-C1, and LGH-D1) have relatively large temporal variation (**Figures 7** and **8**). The representative of two end members (i.e., LGH-D4 and LGH-F1) shows minor to no variations. There was a shift toward the mixing area before November 2015 for mud pools on the axis and lasted until July 2016, the time of the last visit (**Figure 8**). The northern mud pools LGH-G1 and LGH-G3 emitted more andesitic fluids during April 2016 and May 2016, and went back to its previous condition in June 2016 although the western one, LGH-G3, did not fully recover. The time variation of the dominated source of mud pools on the axis possibly results from response of earthquake activities as indicated in the literature (Bonini et al., 2016; Bonini, 2020; Bonini, 2021). In summary, andesitic fluid dominates the

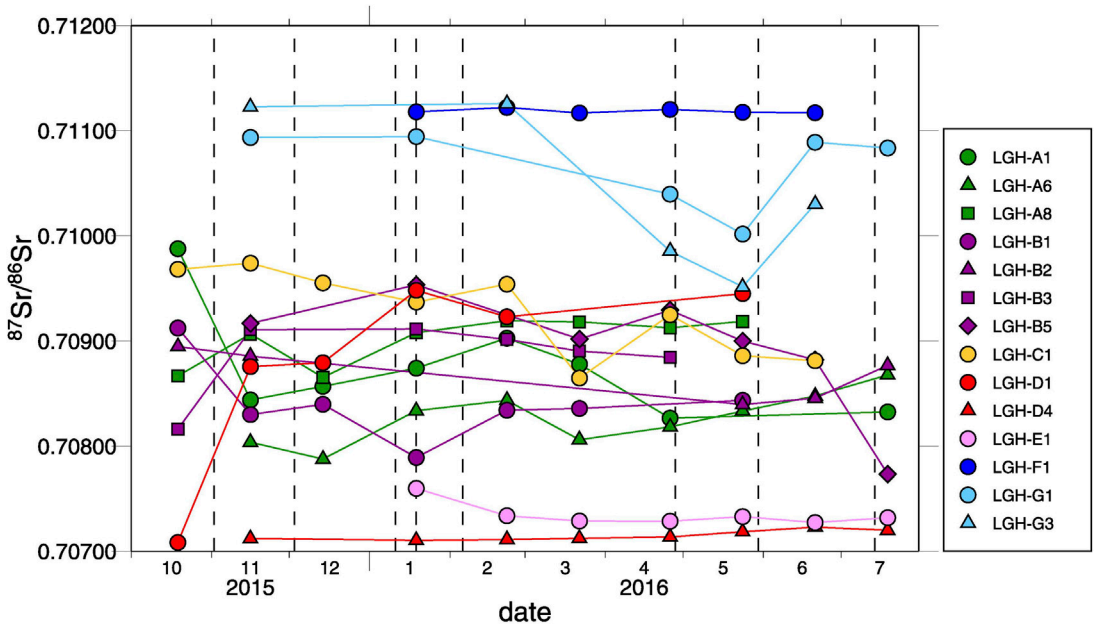

FIGURE 8 | Temporal variation plot of $^{87}Sr/^{86}Sr$ during the sampling period for mud pools which were collected regularly or have long lifetime in MV LGH. Dash lines indicate the dates of earthquakes, which are documented with peak ground acceleration higher than 8 cm/s^2 at the earthquake station approximately 6 km from MV LGH (data from Central Weather Bureau, 2021). The reproducibility is smaller than the symbol. Two end member representatives, LGH-D4 and LGH-F1, have minor variations while others are large.

southeastern region of MV LGH, while sedimentary fluid dominates the northwest. The spatial distribution matches the geological background of the volcanic arc in the east and the forearc basin right beneath and in the west.

The source of low Cl, δD, and $\delta^{18}O$ fluid

Generally speaking, sedimentary MVs have simultaneous low Cl concentration with higher O isotope and lower H isotope relative to seawater, indicating dilution of fresh high $\delta^{18}O$ and low δD water by clay dehydration in the source region (Dählmann and de Lange, 2003; Hensen et al., 2004; You et al., 2004; Chen et al., 2020). MVs in western Taiwan emit fluids of classical geochemical characteristics (You et al., 2004; Yeh et al., 2005; Chao et al., 2011; Chao et al., 2013). However, eastern Taiwan MVs contain fluid of both chloride concentration and water isotopes lower than seawater, indicating different mechanisms or fluid source compared with those of the western ones. Considering the hypothesis that MV fluid originates from altered ancient marine pore water, several possible mechanisms, such as meteoric water input, clay dehydration, or water–rock interaction may be involved in altering the pore water.

Marine pore water originally recorded chemical and isotopic composition of the seawater at the time sediment deposited. As the depth, pressure, and temperature increased, the chemical and isotopic composition of the pore water was altered by early diagenesis, the addition of lateral transport fluids or diffusive/advective fluid migrated from deep underneath (e.g., Kopf, 2002; Aloisi et al., 2004; Hensen et al., 2004; Mazzini and Etiope, 2017; Chen et al., 2020). Lichi Mélange, which is the most likely formation where the fluid source is located, is estimated to be deposited from 5 to 6 Ma (Lin et al., 2019). The $\delta^{18}O$ value of the ancient seawater at that time estimated by benthic foraminifer is about 0.2‰–1.0‰ lower than the present value (Zachos et al., 2008; Lear et al., 2015). This result seems to be a reasonable explanation for water isotope compositions of eastern Taiwan MV fluids since the average $\delta^{18}O$ values are −0.55 and −1.27‰ for LS-A1 and LGH, respectively. However, the preservation of original deposited seawater cannot explain the lowering of the chloride concentration and the enrichment of Ca. Chloride has a very long residence time in seawater (87 million years; Berner and Berner, 1987), indicating limited chloride variation in this time scale. The temporal variation of chloride between 5 and 6 Ma, and the present time is too small to be detected by our quantification precision.

Marine pore waters which show similar chemical and isotopic pattern to eastern Taiwan MV fluids are reported in the literature (Perry et al., 1976; Lawrence et al., 1979; Lawrence and Gieskes, 1981; Gieskes et al., 1990; Gieskes et al., 1993; Kastner et al., 1993). They contain lower Cl, Mg, K, δD, and $\delta^{18}O$ but higher Ca relative to seawater. This pattern is interpreted as low-temperature alternation of volcanic ashes and underlying basaltic ocean crust coupled with diffusive exchange with overlying ocean column (Garlick and Dymond, 1970; Lawrence and Gieskes, 1981). Although the major pattern matches, the slope of oxygen isotope decreasing versus chloride decreasing and calcium increasing are different. Adopting the regression trend established by DSDP cores (Lawrence and Gieskes, 1981) to MV LGH, $\delta^{18}O$ value will have an end member of −7‰ or −12‰ based on the Ca

TABLE 1 | End-member composition of Lei-Gong-Huo (LGH) fluid, the average composition of Luo-Shan (LS)-A1 is also listed for reference.

	pH	Cl^-(mM)	TA (mM)	Na (mM)	Ca (mM)	B (mM)	K (mM)	Mg (mM)	Sr (μM)	S (μM)	Li (μM)	Ba (μM)	$^{87}Sr/^{86}Sr$	$\delta^{88}Sr$ (‰)	δD (‰)	$\delta^{18}O$ (‰)	K/Na (°C)	K/Mg (°C)	Na/K (°C)
LGH-sedimentary	6.87[a]	331[a]	3.34[b]	289[b]	15.7[c]	0.162[c]	0.696[a]	7.60[a]	471[b]	12.9[c]	84.3[b]	424[a]	0.71132[b]	0.22[c]	-4.5[a]	-1.50[a]	63	56	89
LGH-igneous	6.55[d]	334[d]	0.845[e]	141[e]	98.6[f]	1.57[f]	0.635[d]	2.41[d]	112[e]	80.1[f]	26.2[e]	69.6[d]	0.70710[e]	0.37[f]	-4.0[d]	-1.60[d]	86	67	97
LS-A1[g]	7.00	215	0.535	119	46.9	0.979	0.335	0.253	67.4	36.4	11.8	5.14	0.70678	0.32	−2.7	−0.55	67	78	91
Andesite basement[h]	—	—	—	—	—	—	—	—	—	—	—	—	0.70431[h]	0.30[i]	—	—	—	—	—

Note. [a]*Average value of LGH-F and LGH-G samples.*

[b]*Maximum value among LGH-F and LGH-G samples.*

[c]*Minimum value among LGH-F and LGH-G samples.*

[d]*Average value of LGH-D4 and LGH-E samples.*

[e]*Minimum value among LGH-D4 and LGH-E samples.*

[f]*Maximum value among LGH- D4 and LGH-E samples.*

[g]*Average value of LS-A1 samples.*

[h]*The average value of Coastal Range andesite samples adopted from Chen et al. (1990) and Bentahila et al. (2008).*

[i]*The average value of andesite standard AGV-1 (Chanlier et al., 2012) and arc/back-arc hydrothermal fluids (Yoshimura et al., 2020).*

concentration or Ca/Cl ratio respectively. The end-member calculation based on Ca and Ca/Cl ratio of LS-A1 is −3‰ and −9‰, respectively. These end members show lower $\delta^{18}O$ than MV fluids and indicate that $\delta^{18}O$ of eastern Taiwan MV fluid is not simply controlled by water–rock interaction of ancient seawater and volcanic materials. A third mechanism or an additional source of the fluid has to be involved. Considering the Cl concentration of the MV fluids is relatively lower than that of marine pore water showing similar characteristics, this mechanism or additional fluid has to dilute the MV fluids.

Meteoric water is one of the possibilities, and it was previously interpreted as a possible source of eastern Taiwan MV fluid (Yeh et al., 2005). The water isotope values of LGH fall right on the local meteoric water line, and the values of LS only deviated a little from the line (**Figure 6**), making the interpretation look reasonable. However, neither the direct dilution with seawater nor ancient marine pore water by the weighted mean value of meteoric water (Peng et al., 2010) result in the value of the MV fluids. MV LS has a lower chloride concentration but a higher $\delta^{18}O$ relative to LGH, showing conflicting results to meteoric water input. Moreover, water isotopes of meteoric water have strong seasonal variation (Peng et al., 2010), but most fluids from individual mud pools reveal minor temporal variation. Indeed, a diluted sample, LGH-G6_2016–3, is affected by meteoric water input but it is not the major source of MV fluid.

Clay dehydration is one of the common fluid sources for both marine and terrestrial MVs (e.g., Dählmann and de Lange, 2003; Hensen et al., 2004; Chao et al., 2013; Chen et al., 2020). The formation temperature of the eastern Taiwan MV fluids is estimated by major elements (Chao et al., 2011; this study), the existence of the thermogenic methane and equilibrium temperature estimated by methane clumped isotopes of MV LS-A1 (76°C –101°C; Lin et al., 2019) indicate that the source region has reached the temperature of smectite to illite transformation (40°C –150°C; Freed and Peacor, 1989; Ijiri et al., 2018). The addition of clay dehydration fluid leads to the dilution of chloride but increases $\delta^{18}O$ of the MV fluids. This back and forth scenario neither exceeds present seawater value nor MVs in western Taiwan possibly due to a lower degree of dehydration induced by a lower formation temperature (Chao et al., 2011). The large quantify of smectite distributed in present forearc basin (Nayak et al., 2021) indicates sufficient source of fresh water, even the degree of dehydration is low.

In summary, oxygen isotope in eastern Taiwan MV fluids originates from the ancient seawater approximately 5–6 Ma carrying $\delta^{18}O$ values lower than the present value (−0.2‰–1.0‰), decreased by water–rock interaction with volcanic ashes or andesitic basement, and increased by clay dehydration fluid coupled with further chloride dilution.

Water isotopes of LGH fluid show an evaporation trend with the slope close to 2. Normally, the slope of local evaporation line of surface water is around 4 to 5 for normal temperature and humidity conditions. The slope increases with decreasing temperature but no clear relationship with humidity (e.g., Gibson et al., 2008). The surface temperature of eastern Taiwan MV fluids is similar to or only a little higher than the air temperature, from 18°C to 36°C (**Supplementary Table S1**).

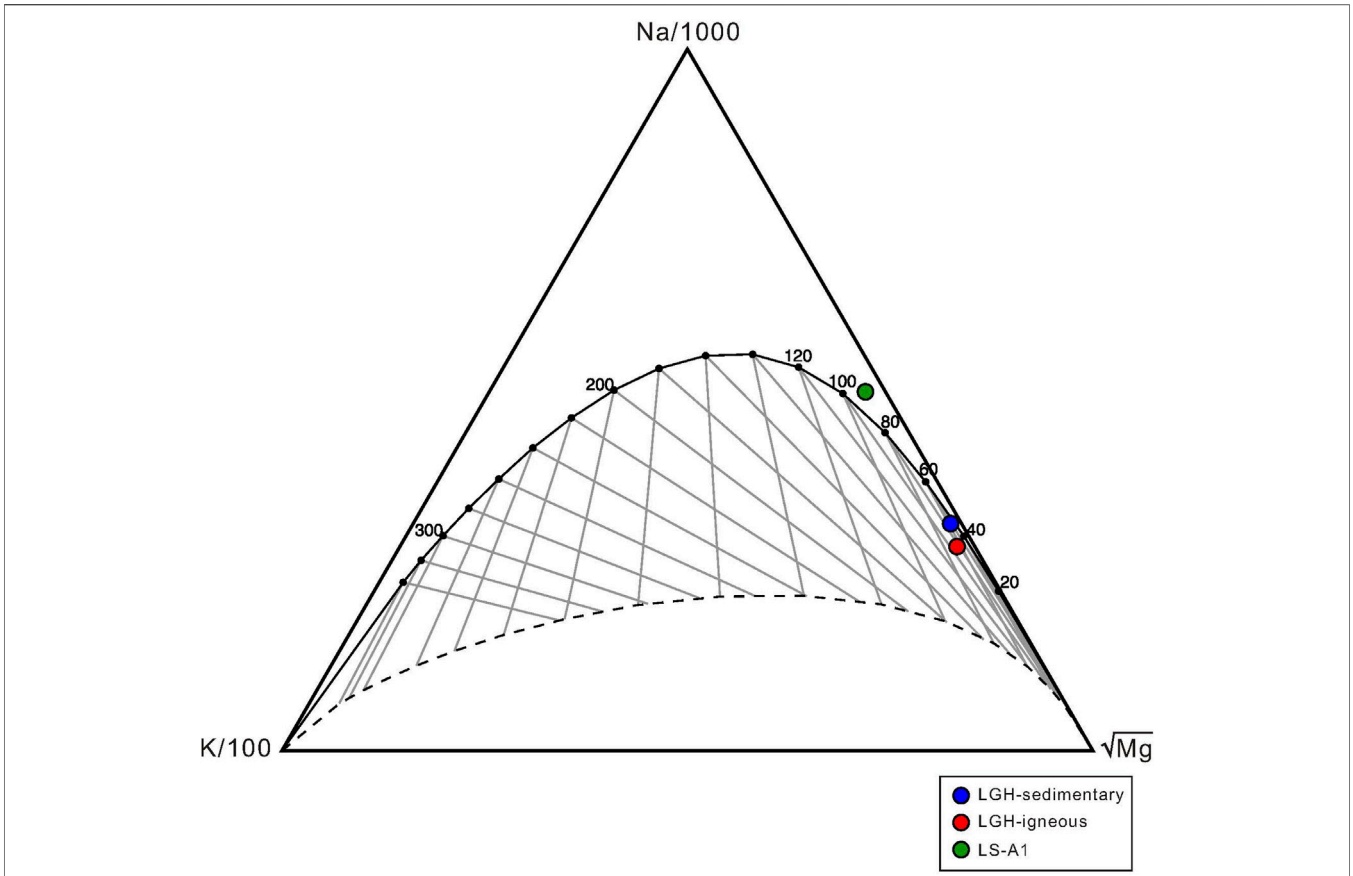

FIGURE 9 | Plot of Giggenbach Na-K-Mg ternary diagram. Solid curve denotes full equilibrium and dash line denotes lower limit of partial equilibrium. Two end members in MV LGH as well as MV LS-A1 fall on or close to full equilibrium.

The reasonable slope of this temperature is approximately from 3.0 to 4.5 for the surface water (Gibson et al., 2008), still higher than the observed slope. However, a similar slope has been documented for soil moisture (Dincer et al., 1974). The evaporation fractionation of MV fluids may have similar behavior to soil moisture.

Geochemical characteristic of two end members in mud volcano Lei-Gong-Huo

Due to strong negative correlation between Na and Ca concentration of the LGH fluid, the end-member composition of sedimentary and igneous fluids can be estimated by the relationship between elements and Na or Ca. Groups F and G are the candidates of sedimentary fluid, while group E and mud pool D4 are the candidates of the igneous fluid. The maximum values of elements which have high positive correlation ($r > 0.65$; **Supplementary Table S2**) with Na or Ca are chosen among candidates as the end-member composition, and the minimum values of elements with high negative correlation ($r < -0.65$) are chosen among candidates. The average values are used for those which have low correlation such as Cl^-, K, Ba, and so on. Samples fractionated by evaporation are excluded for the average value of $\delta^{18}O$ and δD. The estimated end-member composition of the two fluids is listed in **Table 1**.

Besides the high Na concentration and $^{87}Sr/^{86}Sr$ ratio, sedimentary fluid shows significantly high total alkalinity, Sr, Mg, Ba, and Li with low S, Ca, B, and $\delta^{88}Sr$ relative to igneous fluid. B concentration in MV fluids is majorly controlled by readsorption by clay minerals (Chao et al., 2011). The sedimentary fluid has end member concentration of B almost an order lower than igneous fluids, possibly resulting from intense adsorption of B and indicating more sorbent presented in the sedimentary fluid-dominated reservoir. Total alkalinity in the MV fluids generally correlated strongly with CO_2 content of emitted gas (Chao et al., 2010; Lavrushin et al., 2015). Higher alkalinity in the sedimentary end member probably indicates it emits gas with higher CO_2 concentration compared with igneous mud pools. Unfortunately, the gas samples were not collected in this study, and the gas composition data in the literatures were collected from the mud pools on the axis, which are mostly dominated by igneous end member. MV LS-A1 shows total alkalinity concentration lower than LGH and emits lesser CO_2 gas as well (Yang et al., 2004; Chao et al., 2010; Sano et al., 2017), supporting the hypothesis of sedimentary-dominated mud pools in LGH emitting more CO_2.

Calcium and sulfur have interestingly strong positive correlation ($r > 0.99$; **Supplementary Table S2**; **Figure 3**), but they have three orders of magnitude differences in concentration. Anaerobic oxidation of methane (AOM) is the major sink of the sulfur in MV fluids (e.g., Chang et al., 2012) and significantly decreased below pH 7 at salinities below 20‰ (Nauhaus et al., 2005). Indeed, igneous end member has lower pH value than sedimentary end-member (**Table 1**), and sulfur has a moderate negative correlation with pH, indicating sedimentary end member may have stronger AMO and result in lower dissolved S content. However, dissolved sulfate and sulfide were not differentiated in this study because the sulfate concentration is too low to be detected by ion chromatography after dilution. The fundamental mechanism requires further studies.

Stable Sr isotope reveals negative correlation with radiogenic Sr isotope (**Supplementary Table S2**; **Figure 5**). Previous studies indicate that stable Sr isotope in the MVs and other fluids in the hydrosphere may be controlled by the source rock, the degree of water–rock interaction, recrystallization of the carbonates, and coprecipitation with the carbonates (Krabbenhöft et al., 2010; Chao et al., 2013; Voigt et al., 2015; Fruchter et al., 2017; Liu et al., 2017; Voigt et al., 2018; Shao et al., 2021). The coprecipitation is the major factor to fractionate stable Sr isotope in the hydrosphere including seawater, river water, and MV fluids, and raise the $\delta^{88}Sr$ value of the fluid as Sr is removed from the fluid (Krabbenhöft et al., 2010; Chao et al., 2013; Fruchter et al., 2017; Shao et al., 2021). Sedimentary fluid contains higher total alkalinity and lower Ca, resembling carbonate precipitation occurring. However, $\delta^{88}Sr$ and Sr concentration of sedimentary fluid denote a reverse relationship with carbonate precipitation, higher Sr and lower $\delta^{88}Sr$, indicating coprecipitation is not the major factor. The occurrence of clay adsorption increases $\delta^{88}Sr$ of the fluid as well (Liu and You, 2020). Sedimentary fluid has stronger adsorption as indicated by B concentration and $\delta^{11}B$ (Chao et al., 2011), but lower $\delta^{88}Sr$ in the sedimentary fluid expresses a conflicting result. The adsorption is not the major factor, either. The recrystallization of the carbonate releases high $\delta^{88}Sr$ into the fluid (Voigt et al., 2015) but high Sr sedimentary fluid contains low $\delta^{88}Sr$, illustrating it is not the major one. Radiogenic Sr isotope indicates the source of Sr. The stable Sr isotope of the arc basement is not documented and assumed to be similar to andesite standard AGV-1, 0.32‰ (Charlier et al., 2012) or arc/back-arc hydrothermal fluids, 0.29‰–0.30‰ (Yoshimura et al., 2020). Sediments generally have $\delta^{88}Sr$ lower than igneous rock (Halicz et al., 2008; Chao et al., 2015). Both $^{87}Sr/^{86}Sr$ and $\delta^{88}Sr$ of the igneous fluid is higher than that of the andesite basement (**Table 1**; **Figure 4**), indicating incomplete water–rock interaction of the ancient seawater ($^{87}Sr/^{86}Sr = 0.708,925$ to $070,894$; $\delta^{88}Sr = 0.340$ to 0.375; 5 to 6 Ma; DePaolo, 1986; Hodell et al., 1990; Hodell et al., 1991; Paytan et al., 2021) and the andesite basement. With the evidence of negative correlation between radiogenic and stable Sr isotopes of the fluid as well as the source rock, the major fractionation mechanism of $\delta^{88}Sr$ of the LGH fluid is the source.

Chloride, $\delta^{18}O$, and δD show interestingly no discrepancy between two end members. They are relatively conservative parameters and generally are good tracers for water masses. Two end members with distinct Sr isotopes but nearly the same chloride, $\delta^{18}O$ and δD, probably indicate a late stage water–rock interaction before migrating upward. As discussed in *The source of low Cl, δD, and $\delta^{18}O$ fluid* section, the chemical characteristic of chloride and $\delta^{18}O$ in MV LGH was originally ancient seawater. Slightly diluted and lowered $\delta^{18}O$ through interaction with volcanic ashes and/or andesitic basement, and further diluted and raised its $\delta^{18}O$ by clay dehydration. If the clay dehydration occurs after the modification of Sr isotopes, the degree of dehydration or the amount of released fresh water will be different between the two end members because of different lithology, and different lithology implies different quantities of dehydrated minerals. If the degree of clay dehydration or the amount of released fresh water is different between two end members, they should have different chloride concentration and $\delta^{18}O$. On the other hand, $^{87}Sr/^{86}Sr$ is sensitive to water–rock interaction as Sr is easy to be leached out even under low temperature (e.g., Menzies and Seyfried, 1979; James et al., 2003; Ma et al., 2010) but insensitive to smectite to illite transformation because of limited Sr release from the interlayer (e.g., Williams and Hervig, 2005). Fractionation of $\delta^{18}O$ is harder than $^{87}Sr/^{86}Sr$ by water–rock interaction because O has a much larger pool size than Sr (54 M versus 0.2 mM). Thus, the alternation of the Sr isotopes has to occur after clay dehydration to keep H and O isotopes but vary Sr isotopes. The similar Cl, $\delta^{18}O$, and δD indicate two end members suffering similar degree of dehydration in the environment having similar quantity of dehydrated materials. This may imply that the two end members originate from the same source regionally. There are two possibilities to have Sr isotope variation after clay dehydration. One is during fluid migration, the two end members stay in different reservoirs with different lithology and the Sr isotopes are fractionated by the rock they are hosted. The other is after the igneous basement collides into the forearc basin and the fluid interacted with the arc basement has altered its Sr isotopes. The later possibility explains the signal of residual seawater in the sedimentary end member.

In summary, the two end members are likely to be originated at similar depth and formation, undergo similar mechanisms to have their chloride diluted and their water isotopes fractionated. At the final stage before migrating to the surface, their major constitutes and Sr isotopes are further altered by the rock they are hosted. This may occur at the source region or in the reservoir with long residence time.

Formation temperature of the mud volcano fluid

The ratio of dissolved elements is used to estimate the formation temperature of the fluid such as Na/K, K/Na, K/Mg, Mg/Li, and Na/Li ratios (Giggenbach, 1988; Kharaka and Mariner, 1989; Verma and Santoyo, 1997; Can, 2002). Giggenbach (1988) proposes the "Giggenbach ternary diagram" to estimate the equilibrium condition. If the temperature estimated by the K/Na ratio shows similar result to the K/Mg ratio, the fluid is in equilibrium condition. If two temperature estimations have different results, the fluid is in partial equilibrium or immature condition. However, these geothermometer calculations cannot be applied to the fluids that result from the mixing of multiple sources (e.g., Nicholson, 1993). Since at least two fluid sources can be

defined in MV LGH, as discussed above, the temperature calculation is only applied to the end-member composition (**Table 1**). Equations adopted from Giggenbach (1988) and Can (2002) were used:

$$T\ (°C) = \frac{1390}{1.75 - \log\frac{K}{Na}} - 273.15 \quad (2)$$

$$T\ (°C) = \frac{4410}{14.0 - \log\frac{K}{Mg}} - 273.15 \quad (3)$$

$$T\ (°C) = \frac{1052}{1 + e^{\left(1.714 \times \log\left(\frac{Na}{K}\right) + 0.252\right)}} + 76 \quad (4)$$

where all element concentrations presented in the above equations are in ppm.

Both end members in LGH show lower K/Mg temperature than K/Na, indicating partial equilibrium of the fluid (**Table 1**; **Figure 9**). Igneous end member has higher formation temperature than sedimentary end member by all three equations. This may imply that the source or the long residence time fluid reservoir of sedimentary end member has shallower depth or lower geothermal gradient than that of igneous end member. The later inference is the likely scenario because of large heat flow variation across the Longitude Valley (Chi and Reed, 2008; Wu et al., 2013). Sedimentary end member in LGH show similar Na–K-based temperature with MV LS-A1. LS-A1 has a reverse relationship between K/Na and K/Mg temperature. Due to shorter equilibrium time of Mg, K/Mg temperature is generally lower than that of K/Na. Therefore, Na–K-based geothermometers are often used to estimate the source temperature, and K/Mg geothermometer is used to estimate the temperature of the shallower reservoir (Giggenbach, 1988; Verma et al., 2008). However, solute geothermometers have an error range between 20°C and 40°C; thus, the 11°C difference still falls within the error range and can be seen as in an equilibrium condition (Verma et al., 2008). These solute geothermometers of MV LS-A1 show similar results to the temperature estimated by methane clump isotopes (Lin et al., 2019), indicating similar source depth of gas and saline water.

Possible geological structure for spatial distribution

Generally speaking, if a fluid contributed by two reservoirs with distinct chemical compositions lies at depth and its chemical composition changes with time; that means fluids from two reservoirs mix well at certain depth, migrate to surface afterward and the contribution from each reservoir changes with time. Even with some split fluid channels near the surface, the chemical composition of the main crater and the satellites will vary together. However, chemical and isotopic compositions of MV LGH show spatial distribution of two-end-member mixing and the mud pools on the axis denote time variation, indicating the fluids from two sources mix close to the surface. Terrestrial MVs are mostly distributed on the geological fracture structure such as faults and the axis of anticlines (Bonini, 2012; Mazzini and Etiope, 2017). Anticline is a reasonable possibility since two sources may migrate from two flanks of the anticline and converge close to the surface. But the flank of the anticline is actually the compression region and only the axis provide the extension condition, the fluid channels probably will not exist in the flanks of the anticline. Furthermore, whether it is a normal anticline or a fault-related anticline, the axis of the fold should be parallel or subparallel to the strike of the strata nearby. Assuming the distribution trend of the mud pools are able to indicate the direction of the fold axis or fault as indicated in the literature (Mazzini and Etiope, 2017), the trend of mud pool distribution in LGH is not parallel to regional strike of strata (Jiang et al., 2011). This anticline hypothesis is not supported by the field work investigation, either. The result of field work investigation indicates the strike–slip fault is the major geological structure in the study area (Lin et al., 2008) and the folds are in a small scale, not likely to extend to the depth. The scattered distribution of mud pools at the northwestern part of MV LGH may indicate that the fracture structure for the underground fluid pathway may result from the fault. The shape of fault rupture on the surface is not a straight line at the outcrop scale; it ruptures irregularly. Large spatial–temporal variation of chemical composition at the northwestern part of LGH (**Figure 3** and **Figure 7**) indicates complex conduits underground. Geodesic evidence reveals that MV LGH is located on the local extension zone (Ching et al., 2007; Lin et al., 2010) and the fluid channels are under unclamping situation coseismically (Bonini et al., 2016; Bonini, 2021). With the spatial distribution of the mud pools and the extension fractures after 2003 Chengkung earthquake ($M_w = 6.8$) recorded by Jiang et al. (2011), each group of mud pools seems to result from underground extensional cracks and provides pathways for the fluids. The fluid channels are probably induced by a local normal fault and the orientation of the mud pools may denote the distribution of the fault zone.

The volcanic and sedimentary hybrid system

MVs in eastern Taiwan are not the typical ones like their counterparts in western Taiwan. They emit gases with low CO_2 (<0.2%), higher N_2 (up to 10%) and He isotopes (up to 1.9 Ra; Yang et al., 2003; Yang et al., 2004; Chao et al., 2010; Sun et al., 2010; Sano et al., 2017), and waters which contain igneous signals illustrated by high Ca/Cl and low $^{87}Sr/^{86}Sr$ ratios (You et al., 2004; Chao et al., 2011; Chao et al., 2013; this study). They also lack the geophysical evidence of mud diapir underneath. The volcanic and sedimentary hybrid system named the sediment-hosted geothermal system has its definition on several gas and isotopic compositions (Procesi et al., 2019). Although MVs in eastern Taiwan do not match all the chemical definitions, we suggest they are still able to be classified into this hybrid system on a position very close to the hydrocarbon sedimentary system (typical sedimentary MVs).

CONCLUSION

A total of 175 water samples emitted from 46 mud pools of MV LGH and 1 mud pool from MV LS in eastern Taiwan were collected monthly in 10 campaigns, and their dissolved major and trace ion/element compositions as well as O, H, and Sr isotope ratios were analyzed. The results of chemical compositions and isotope ratios agree with the limited previous findings (You et al., 2004; Yeh et al., 2005; Chao et al., 2011; Chang et al., 2012; Chao et al., 2013). Our major results are summarized as follows:

1. The chemical compositions of MV fluids in eastern Taiwan are dominated by Cl, Ca, and Na. In MV LGH, the spatial variation of Na, Ca, Mg, B, and Sr isotopes is large. At least two fluid sources can be identified by its chemical characteristic. High Na, Li, total alkalinity, $^{87}Sr/^{86}Sr$, but low Ca, S, B, and $\delta^{88}Sr$ fluid is distributed in the northwest corner and results from water–rock interaction with sediments. Another fluid with reversed chemical characteristic, high Ca, S, B, and $\delta^{88}Sr$ with low Na and $^{87}Sr/^{86}Sr$, is located in the southeast corner, implying water–rock interaction with andesitic arc basement. The rest of the mud pools show mixing behavior between the two sources. However, several sedimentary-dominated mud pools denote no igneous contribution but a mixing trend extrapolating toward seawater, indicating the existence of residual ancient seawater. The composition of two end members is stable during the study period and the mud pools on the axis show temporal variation.
2. Fluids from both MVs present chloride, O, and H isotopes lower than seawater without temporal variation and mud pools in LGH show limited spatial variation. With the evidence of Ca enrichment and $^{87}Sr/^{86}Sr$, a three-step model of fluid origination is proposed. Eastern Taiwan MV fluids are initially ancient seawater, preserved in the pore space of the sediment, and its chemical and isotopic composition is altered by water–rock interaction with volcanic ashes by slightly diluting the chloride concentration, great enrichment of Ca, and lowering the O and H isotopes like deep marine pore water worldwide. As the temperature increases, probably due to the arc collision, clay dehydration occurs. The most likely clay dehydration is smectite to illite transformation, and it leads to further dilution of chloride but raises the $\delta^{18}O$ of the fluid. This increase is small and does not exceed the current seawater value, corresponding to lower formation temperature estimated by the solute geothermometer compared with MV fluids from western Taiwan. For the fluid in LGH, the chemical composition and Sr isotopes are further modified by the ambient rock of the source region or the long residence time fluid reservoir before ascending to the surface. This final stage modification changes neither the chloride concentration nor the O isotopes of the fluid.
3. Stable Sr isotopes, $\delta^{88}Sr$, show strong negative correlation with $^{87}Sr/^{86}Sr$ ($r = -0.81$). This evidence indicates that the major factor to fractionation $\delta^{88}Sr$ of the water expelled by eastern Taiwan MVs is the source. Igneous rocks have relatively low $^{87}Sr/^{86}Sr$ and high $\delta^{88}Sr$ while sediments have relatively high $^{87}Sr/^{86}Sr$ and low $\delta^{88}Sr$.
4. Based on spatial distribution of the mud pools and two chemical end members as well as the orientation of the local strata and geological structures, the hypothesis of local extension-induced normal fault provided pathway is suggested for MV LGH.

This study indicates the importance and the robustness of Sr isotopes as the source and reservoir tracer for MV fluids. Chloride concentration, H, and O isotopes are easily masked by evaporation and fresh surface water input but $^{87}Sr/^{86}Sr$ has limited influence from those factors. H and O can be the tracer of regional source, and MV water from different reservoirs may have similar to the same O isotopes but quite different $^{87}Sr/^{86}Sr$ ratios.

DATA AVAILABILITY STATEMENT

The original contributions presented in the study are included in the article/**Supplementary Material**. further inquiries can be directed to the corresponding author.

AUTHOR CONTRIBUTIONS

H-CC contributed to the conception and design of the study and wrote the first draft of the manuscript. H-CC and C-CH did the field work. C-FY and H-CL provided the instrumental resources. H-CC and I-TL performed the chemical and isotopic measurements. L-HC wrote a section of the manuscript. H-CL and C-HC performed analytical methods and maintained the instruments. All authors contributed to manuscript revision, read, and approved the submitted version.

FUNDING

This study was supported by the MOST grants MOST107-2116-M-194–007, MOST108-2116-M-194–001, MOST109-2116-M-194–009, and MOST110-2116-M-194–012 to H-CC.

ACKNOWLEDGMENTS

Constructive comments by three reviewers are greatly appreciated, as well as the associate editor, Dr. Zheng, for their effective handling of this manuscript.

SUPPLEMENTARY MATERIAL

The Supplementary Material for this article can be found online at: https://www.frontiersin.org/articles/10.3389/feart.2021.750436/full#supplementary-material

REFERENCES

Alexander Bentley, R. (2006). Strontium Isotopes from the Earth to the Archaeological Skeleton: A Review. *J. Archaeol. Method Theor.* 13, 135–187. doi:10.1007/s10816-006-9009-x

Aloisi, G., Drews, M., Wallmann, K., and Bohrmann, G. (2004). Fluid Expulsion from the Dvurechenskii Mud Volcano (Black Sea)Part I. Fluid Sources and Relevance to Li, B, Sr, I and Dissolved Inorganic Nitrogen Cycles. *Earth Planet. Sci. Lett.* 225, 347–363. doi:10.1016/s0012-821x(04)00415-7

Banner, J. L. (2004). Radiogenic Isotopes: Systematics and Applications to Earth Surface Processes and Chemical Stratigraphy. *Earth-Sci. Rev.* 65, 141–194. doi:10.1016/S0012-8252(03)00086-2

Bentahila, Y., Ben Othman, D., and Luck, J.-M. (2008). Strontium, lead and Zinc Isotopes in marine Cores as Tracers of Sedimentary Provenance: A Case Study Around Taiwan Orogen. *Chem. Geol.* 248, 62–82. doi:10.1016/j.chemgeo.2007.10.024

Berner, E. K., and Berner, R. A. (1987). *The Global Water Cycle: Geochemistry Environment*. New Jersey: Prentice-Hall Inc.

Bonini, M., Rudolph, M. L., and Manga, M. (2016). Long- and Short-Term Triggering and Modulation of Mud Volcano Eruptions by Earthquakes. *Tectonophysics* 672-673, 190–211. doi:10.1016/j.tecto.2016.01.037

Bonini, M. (2012). Mud Volcanoes: Indicators of Stress Orientation and Tectonic Controls. *Earth-Science Rev.* 115, 121–152. doi:10.1016/j.earscirev.2012.09.002

Bonini, M. (2020). Investigating Earthquake Triggering of Fluid Seepage Systems by Dynamic and Static Stresses. *Earth-Sci. Rev.* 210, 103343. doi:10.1016/j.earscirev.2020.103343

Bonini, M. (2021). Structural Controls and Earthquake Response of Taiwan Mud Volcanoes. *Mar. Pet. Geol.* 128, 105050. doi:10.1016/j.marpetgeo.2021.105050

Bray, C. J., and Karig, D. E. (1985). Porosity of Sediments in Accretionary Prisms and Some Implications for Dewatering Processes. *J. Geophys. Res.* 90, 768–778. doi:10.1029/JB090iB01p00768

Bujakaite, M. I., Lavrushin, V. Y., and Pokrovsky, B. G. (2019). Strontium Isotope Composition of Mud Volcanic Waters in Azerbaijan. *Lithol. Miner. Resour.* 54, 351–361. doi:10.1134/S0024490219050031

Can, I. (2002). A New Improved Na/K Geothermometer by Artificial Neural Networks. *Geothermics* 31, 751–760. doi:10.1016/S0375-6505(02)00044-5

Central Weather Bureau (2021). *Seismological Center earthquake information*. Available at: https://scweb.cwb.gov.tw/en-us/earthquake/data (Accessed June 10, 2021).

Chang, C.-P., Angelier, J., and Huang, C.-Y. (2000). Origin and Evolution of a Mélange: the Active Plate Boundary and Suture Zone of the Longitudinal Valley, Taiwan. *Tectonophysics* 325, 43–62. doi:10.1016/S0040-1951(00)00130-X

Chang, Y.-H., Cheng, T.-W., Lai, W.-J., Tsai, W.-Y., Sun, C.-H., Lin, L.-H., et al. (2012). Microbial Methane Cycling in a Terrestrial Mud Volcano in Eastern Taiwan. *Environ. Microbio.* 14 (4), 895–908. doi:10.1111/j.1462-2920.2011.02658.x

Chao, H.-C., You, C.-F., and Sun, C.-H. (2010). Gases in Taiwan Mud Volcanoes: Chemical Composition, Methane Carbon Isotopes, and Gas Fluxes. *Appl. Geochem.* 25, 428–436. doi:10.1016/j.apgeochem.2009.12.009

Chao, H.-C., You, C.-F., Wang, B.-S., Chung, C.-H., and Huang, K.-F. (2011). Boron Isotopic Composition of Mud Volcano Fluids: Implications for Fluid Migration in Shallow Subduction Zones. *Earth Planet. Sci. Lett.* 305, 32–44. doi:10.1016/j.epsl.2011.02.033

Chao, H.-C., You, C.-F., Liu, H.-C., and Chung, C.-H. (2013). The Origin and Migration of Mud Volcano Fluids in Taiwan: Evidence from Hydrogen, Oxygen, and Strontium Isotopic Compositions. *Geochim. Cosmochim. Acta* 114, 29–51. doi:10.1016/j.gca.2013.03.035

Chao, H.-C., You, C.-F., Liu, H.-C., and Chung, C.-H. (2015). Evidence for Stable Sr Isotope Fractionation by Silicate Weathering in a Small Sedimentary Watershed in Southwestern Taiwan. *Geochim. Cosmochim. Acta* 165, 324–341. doi:10.1016/j.gca.2015.06.006

Charlier, B. L. A., Nowell, G. M., Parkinson, I. J., Kelley, S. P., Pearson, D. G., and Burton, K. W. (2012). High Temperature Strontium Stable Isotope Behaviour in the Early Solar System and Planetary Bodies. *Earth Planet. Sci. Lett.* 329-330, 31–40. doi:10.1016/j.epsl.2012.02.008

Chen, C. H., Shieh, Y. N., Lee, T., Chen, C. H., and Mertzman, S. A. (1990). Nd-Sr-O Isotopic Evidence for Source Contamination and an Unusual Mantle Component under Luzon Arc. *Geochim. Cosmochim. Acta* 54, 2473–2483. doi:10.1016/0016-7037(90)90234-C

Chen, N.-C., Yang, T. F., Hong, W.-L., Yu, T.-L., Lin, I.-T., Wang, P.-L., et al. (2020). Discharge of Deeply Rooted Fluids from Submarine Mud Volcanism in the Taiwan Accretionary Prism. *Sci. Rep.* 10, 381. doi:10.1038/s41598-019-57250-9

Chi, W.-C., and Reed, D. L. (2008). Evolution of Shallow, Crustal thermal Structure from Subduction to Collision: An Example from Taiwan. *Geol. Soc. America Bull.* 120, 679–690. doi:10.1130/B26210.1

Ching, K.-E., Rau, R.-J., and Zeng, Y. (2007). Coseismic Source Model of the 2003Mw6.8 Chengkung Earthquake, Taiwan, Determined from GPS Measurements. *J. Geophys. Res.* 112, B06422. doi:10.1029/2006JB004439

Ching, K.-E., Rau, R.-J., Johnson, K. M., Lee, J.-C., and Hu, J.-C. (2011). Present-day Kinematics of Active Mountain Building in Taiwan from GPS Observations during 1995-2005. *J. Geophys. Res.* 116, B09405. doi:10.1029/2010JB008058

Dählmann, A., and de Lange, G. J. (2003). Fluid-sediment Interactions at Eastern Mediterranean Mud Volcanoes: A Stable Isotope Study from ODP Leg 160. *Earth Planet. Sci. Lett.* 212, 377–391. doi:10.1016/S0012-821X(03)00227-9

de Souza, G. F., Reynolds, B. C., Kiczka, M., and Bourdon, B. (2010). Evidence for Mass-dependent Isotopic Fractionation of Strontium in a Glaciated Granitic Watershed. *Geochim. Cosmochim. Acta* 74, 2596–2614. doi:10.1016/j.gca.2010.02.012

Delisle, G., von Rad, U., Andruleit, H., von Daniels, C., Tabrez, A., and Inam, A. (2002). Active Mud Volcanoes on- and Offshore Eastern Makran, Pakistan. *Int. J. Earth Sci.* 91, 93–110. doi:10.1007/s005310100203

DePaolo, D. J. (1986). Detailed Record of the Neogene Sr Isotopic Evolution of Seawater from DSDP Site 590B. *Geol.* 14 (2), 103–106. doi:10.1130/0091-7613(1986)14<103:drotns>2.0.co;2

Deville, E., and Guerlais, S.-H. (2009). Cyclic Activity of Mud Volcanoes: Evidences from Trinidad (SE Caribbean). *Mar. Pet. Geol.* 26, 1681–1691. doi:10.1016/j.marpetgeo.2009.03.002

Dia, A. N., Castrec, M., Boulègue, J., and Boudou, J. P. (1995). Major and Trace Element and Sr Isotope Constraints on Fluid Circulations in the Barbados Accretionary Complex. Part 1: Fluid Origin. *Earth Planet. Sci. Lett.* 134, 69–85. doi:10.1016/0012-821X(95)00102-I

Dia, A. N., Castrec-Rouelle, M., Boulègue, J., and Comeau, P. (1999). Trinidad Mud Volcanoes: Where Do the Expelled Fluids Come from? *Geochim. Cosmochim. Acta* 63, 1023–1038. doi:10.1016/S0016-7037(98)00309-3

Dimitrov, L. I. (2002). Mud Volcanoes-The Most Important Pathway for Degassing Deeply Buried Sediments. *Earth-Sci. Rev.* 59, 49–76. doi:10.1016/S0012-8252(02)00069-7

Dincer, T., Al-Mugrin, A., and Zimmermann, U. (1974). Study of the Infiltration and Recharge through the Sand Dunes in Arid Zones with Special Reference to the Stable Isotopes and Thermonuclear Tritium. *J. Hydrol.* 23, 79–109. doi:10.1016/0022-1694(74)90025-0

Douglas, G., Palmer, M., and Caitcheon, G. (2003). "The Provenance of Sediments in Moreton Bay, Australia: a Synthesis of Major, Trace Element and Sr-Nd-Pb Isotopic Geochemistry, Modelling and Landscape Analysis," in *Developments in Hydrobiology* (Dordrecht: Springer), 169, 145–152. doi:10.1007/978-94-017-3366-3_20

Etiope, G., Caracausi, A., Favara, R., Italiano, F., and Baciu, C. (2002). Methane Emission from the Mud Volcanoes of Sicily (Italy). *Geophys. Res. Lett.* 29, 56–61. doi:10.1029/2001GL014340

Etiope, G., Martinelli, G., Caracausi, A., and Italiano, F. (2007). Methane Seeps and Mud Volcanoes in Italy: Gas Origin, Fractionation and Emission to the Atmosphere. *Geophys. Res. Lett.* 34. doi:10.1029/2007GL030341

Etiope, G., Feyzullayev, A., and Baciu, C. L. (2009). Terrestrial Methane Seeps and Mud Volcanoes: A Global Perspective of Gas Origin. *Mar. Pet. Geology.* 26, 333–344. doi:10.1016/j.marpetgeo.2008.03.001

Etiope, G., Baciu, C. L., and Schoell, M. (2011a). Extreme Methane Deuterium, Nitrogen and Helium Enrichment in Natural Gas from the Homorod Seep (Romania). *Chem. Geol.* 280, 89–96. doi:10.1016/j.chemgeo.2010.10.019

Etiope, G., Nakada, R., Tanaka, K., and Yoshida, N. (2011b). Gas Seepage from Tokamachi Mud Volcanoes, Onshore Niigata Basin (Japan): Origin, post-genetic Alterations and CH4-CO2 Fluxes. *Appl. Geochem.* 26, 348–359. doi:10.1016/j.apgeochem.2010.12.008

Farhadian Babadi, M., Mehrabi, B., Tassi, F., Cabassi, J., Vaselli, O., Shakeri, A., et al. (2019). Origin of Fluids Discharged from Mud Volcanoes in SE Iran. *Mar. Pet. Geology.* 106, 190–205. doi:10.1016/j.marpetgeo.2019.05.005

Farhadian Babadi, M., Mehrabi, B., Tassi, F., Cabassi, J., Pecchioni, E., Shakeri, A., et al. (2021). Geochemistry of Fluids Discharged from Mud Volcanoes in SE Caspian Sea (Gorgan Plain, Iran). *Int. Geology. Rev.* 63, 437–452. doi:10.1080/00206814.2020.1716400

Fortunato, G., Mumic, K., Wunderli, S., Pillonel, L., Bosset, J. O., and Gremaud, G. (2004). Application of Strontium Isotope Abundance Ratios Measured by MC-ICP-MS for Food Authentication. *J. Anal. Spectrom.* 19, 227–234. doi:10.1039/B307068A

Freed, R. L., and Peacor, D. R. (1989). Variability in Temperature of the Smectite/Illite Reaction in Gulf Coast Sediments†. *Clay Minerals* 24, 171–180. doi:10.1180/claymin.1989.024.2.05

Fruchter, N., Lazar, B., Nishri, A., Almogi-Labin, A., Eisenhauer, A., Be'eri Shlevin, Y., et al. (2017). 88 Sr/86 Sr Fractionation and Calcite Accumulation Rate in the Sea of Galilee. *Geochim. Cosmochim. Acta* 215, 17–32. doi:10.1016/j.gca.2017.07.026

Garlick, G. D., and Dymond, J. R. (1970). Oxygen Isotope Exchange between Volcanic Materials and Ocean Water. *Geol. Soc. America Bull.* 81 (7), 2137–2142. doi:10.1130/0016-7606(1970)81[2137:oiebvm]2.0.co;2

Gibson, J. J., Birks, S. J., and Edwards, T. W. D. (2008). Global Prediction ofδAandδ2H-δ18O Evaporation Slopes for Lakes and Soil Water Accounting for Seasonality. *Glob. Biogeochem. Cycles* 22. doi:10.1029/2007GB002997

Gieskes, J. M., Kastner, M., and Warner, T. B. (1975). Evidence for Extensive Diagenesis, Madagascar Basin, Deep Sea Drilling Site 245. *Geochim. et Cosmochim. Acta* 39, 1385–1393. doi:10.1016/0016-7037(75)90117-9

Gieskes, J. M., Vrolijk, P., and Blanc, G. (1990). Hydrogeochemistry of the Northern Barbados Accretionary Complex Transect: Ocean Drilling Project Leg 110. *J. Geophys. Res.* 95, 8809–8818. doi:10.1029/JB095iB06p08809

Gieskes, J. M., Gamo, T., and Kastner, M. (1993). Major and Minor Element Geochemistry of Interstitial Waters of Site 808, Nankai Trough: An Overview. *Proc. ODP. Sci. Results* 131, 387–396. doi:10.2973/odp.proc.sr.131.133.1993

Giggenbach, W. F. (1988). Geothermal Solute Equilibria. Derivation of Na-K-Mg-Ca Geoindicators. *Geochim. Cosmochim. Acta* 52, 2749–2765. doi:10.1016/0016-7037(88)90143-3

Halicz, L., Segal, I., Fruchter, N., Stein, M., and Lazar, B. (2008). Strontium Stable Isotopes Fractionate in the Soil Environments? *Earth Planet. Sci. Lett.* 272, 406–411. doi:10.1016/j.epsl.2008.05.005

Henderson, P. (1982). *Inorganic Geochemistry*. New York: Pergamon Press.

Hensen, C., Wallmann, K., Schmidt, M., Ranero, C. R., and Suess, E. (2004). Fluid Expulsion Related to Mud Extrusion off Costa Rica-A Window to the Subducting Slab. *Geol* 32, 201–204. doi:10.1130/G20119.1

Hodell, D. A., Mead, G. A., and Mueller, P. A. (1990). Variation in the Strontium Isotopic Composition of Seawater (8 Ma to Present) : Implications for Chemical Weathering Rates and Dissolved Fluxes to the Oceans. *Chem. Geology. Isotope Geosci. section* 80, 291–307. doi:10.1016/0168-9622(90)90011-Z

Hodell, D. A., Mueller, P. A., and Garrido, J. R. (1991). Variations in the Strontium Isotopic Composition of Seawater during the Neogene. *Geol* 19 (1), 24–27. doi:10.1130/0091-7613(1991)019<0024:vitsic>2.3.co;2

Ijiri, A., Tomioka, N., Wakaki, S., Masuda, H., Shozugawa, K., Kim, S., et al. (2018). Low-temperature clay mineral Dehydration Contributes to Porewater Dilution in Bering Sea Slope Subseafloor. *Front. Earth Sci.* 6, 36. doi:10.3389/feart.2018.00036

James, R. H., Allen, D. E., and Seyfried, W. E. (2003). An Experimental Study of Alteration of Oceanic Crust and Terrigenous Sediments at Moderate Temperatures (51 to 350°C): Insights as to Chemical Processes in Near-Shore ridge-flank Hydrothermal Systems. *Geochim. Cosmochim. Acta* 67, 681–691. doi:10.1016/S0016-7037(02)01113-4

Jiang, G.-J., Angelier, J., Lee, J.-C., Chu, H.-T., Hu, J.-C., and Mu, C.-H. (2011). Faulting and Mud Volcano Eruptions inside of the Coastal Range during the 2003 Mw = 6.8 Chengkung Earthquake in Eastern Taiwan. *Terr. Atmos. Ocean. Sci.* 22, 463–473. doi:10.3319/tao.2011.04.22.01(tt)

Kastner, M., Elderfield, H., Jenkins, W. J., Gieskes, J. M., and Gamo, T. (1993). Geochemical and Isotopic Evidence for Fluid Flow in the Western Nankai Subduction Zone, Japan. *Proc. ODP. Sci. Results* 131, 397–413. doi:10.2973/odp.proc.sr.131.143.1993

Kharaka, Y. K., and Mariner, R. H. (1989). *Chemical Geothermometers and Their Applications to Formation Waters from Sedimentary Basins, Thermal History of Sedimentary Basins: Methods and Case Histories*. New York: Springer, 99–117. doi:10.1007/978-1-4612-3492-0_6

Kopf, A., and Deyhle, A. (2002). Back to the Roots: boron Geochemistry of Mud Volcanoes and its Implications for Mobilization Depth and Global B Cycling. *Chem. Geol.* 192, 195–210. doi:10.1016/S0009-2541(02)00221-8

Kopf, A. J. (2002). Significance of Mud Volcanism. *Rev. Geophys.* 40, 2–1. doi:10.1029/2000RG000093

Krabbenhöft, A., Fietzke, J., Eisenhauer, A., Liebetrau, V., Böhm, F., and Vollstaedt, H. (2009). Determination of Radiogenic and Stable Strontium Isotope Ratios (87Sr/86Sr; δ88/86Sr) by thermal Ionization Mass Spectrometry Applying an 87Sr/84Sr Double Spike. *J. Anal. Spectrom.* 24, 1267–1271. doi:10.1039/B906292K

Krabbenhöft, A., Eisenhauer, A., Böhm, F., Vollstaedt, H., Fietzke, J., Liebetrau, V., et al. (2010). Constraining the marine Strontium Budget with Natural Strontium Isotope Fractionations (87Sr/86Sr*, δ88/86Sr) of Carbonates, Hydrothermal Solutions and River Waters. *Geochim. Cosmochim. Acta* 74, 4097–4109. doi:10.1016/j.gca.2010.04.009

Lavrushin, V. Y., Kopf, A., Deyhle, A., and Stepanets, M. I. (2003). Formation of Mud-Volcanic Fluids in Taman (Russia) and Kakhetia (Georgia): Evidence from Boron Isotopes. *Lithol. Miner. Resour.* 38, 120–153. doi:10.1023/A:1023452025440

Lavrushin, V. Y., Dubinina, E. O., and Avdeenko, A. S. (2005). Isotopic Composition of Oxygen and Hydrogen in Mud-Volcanic Waters from Taman (Russia) and Kakhetia (Eastern Georgia). *Lithol. Miner. Resour.* 40, 123–137. doi:10.1007/s10987-005-0014-z

Lavrushin, V. Y., Guliev, I. S., Kikvadze, O. E., Aliev, A. A., Pokrovsky, B. G., and Polyak, B. G. (2015). Waters from Mud Volcanoes of Azerbaijan: Isotopic-Geochemical Properties and Generation Environments. *Lithol. Miner. Resour.* 50, 1–25. doi:10.1134/S0024490215010034

Lawrence, J. R., and Gieskes, J. M. (1981). Constraints on Water Transport and Alteration in the Oceanic Crust from the Isotopic Composition of Pore Water. *J. Geophys. Res.* 86, 7924–7934. doi:10.1029/JB086iB09p07924

Lawrence, J. R., Drever, J. I., Anderson, T. F., and Brueckner, H. K. (1979). Importance of Alteration of Volcanic Material in the Sediments of Deep Sea Drilling Site 323: Chemistry, and. *Geochim. Cosmochim. Acta* 43, 573–588. doi:10.1016/0016-7037(79)90166-2

Lear, C. H., Coxall, H. K., Foster, G. L., Lunt, D. J., Mawbey, E. M., Rosenthal, Y., et al. (2015). Neogene Ice Volume and Ocean Temperatures: Insights from Infaunal Foraminiferal Mg/Ca Paleothermometry. *Paleoceanography* 30, 1437–1454. doi:10.1002/2015PA002833

Li, Y.-H. (1976). Denudation of Taiwan Island since the Pliocene Epoch. *Geol* 4, 105–106. doi:10.1130/0091-7613(1976)4<105:dotist>2.0.co;2

Lin, C. T., Harris, R., Sun, W. D., and Zhang, G. L. (2019). Geochemical and Geochronological Constraints on the Origin and Emplacement of the East Taiwan Ophiolite. *Geochem. Geophys. Geosyst.* 20, 2110–2133. doi:10.1029/2018GC007902

Lin, W. H., Lin, C. W., Liu, Y. C., and Chen, P. T. (2008). *Explanatory Text for the Geologic Map of Taiwan: Taitung and Jhihben Sheet Scale 1:50,000*. Taipei, Taiwan: Central Geological Survey, MOEA.

Lin, K.-C., Hu, J.-C., Ching, K.-E., Angelier, J., Rau, R.-J., Yu, S.-B., et al. (2010). GPS Crustal Deformation, Strain Rate, and Seismic Activity after the 1999 Chi-Chi Earthquake in Taiwan. *J. Geophys. Res.* 115, B07404. doi:10.1029/2009JB006417

Liu, H.-C., and You, C.-F. (2020). Stable Sr Isotope Fractionation between Fluids and clay Minerals: Insight from Laboratory Batch Experiments. *Goldschmidt Abstr.*, 1590. doi:10.46427/gold2020.1590

Liu, H.-C., You, C.-F., Chung, C.-H., Huang, K.-F., and Liu, Z.-F. (2011). Source Variability of Sediments in the Shihmen Reservoir, Northern Taiwan: Sr Isotopic Evidence. *J. Asian Earth Sci.* 41, 297–306. doi:10.1016/j.jseaes.2011.02.013

Liu, H.-C., You, C.-F., Huang, K.-F., and Chung, C.-H. (2012). Precise Determination of Triple Sr Isotopes (δ87Sr and δ88Sr) Using MC-ICP-MS. *Talanta* 88, 338–344. doi:10.1016/j.talanta.2011.10.050

Liu, H.-C., You, C.-F., Zhou, H., Huang, K.-F., Chung, C.-H., Huang, W.-J., et al. (2017). Effect of Calcite Precipitation on Stable Strontium Isotopic Compositions: Insights from Riverine and Pool Waters in a Karst Cave. *Chem. Geology.* 456, 85–97. doi:10.1016/j.chemgeo.2017.03.008

Ma, J., Wei, G., Xu, Y., and Long, W. (2010). Variations of Sr-Nd-Hf Isotopic Systematics in basalt during Intensive Weathering. *Chem. Geology.* 269, 376–385. doi:10.1016/j.chemgeo.2009.10.012

Mazzini, A., and Etiope, G. (2017). Mud Volcanism: An Updated Review. *Earth-Sci. Rev.* 168, 81–112. doi:10.1016/j.earscirev.2017.03.001

Mazzini, A., Svensen, H., Akhmanov, G. G., Aloisi, G., Planke, S., Malthe-Sørenssen, A., et al. (2007). Triggering and Dynamic Evolution of the LUSI Mud Volcano, Indonesia. *Earth Planet. Sci. Lett.* 261, 375–388. doi:10.1016/j.epsl.2007.07.001

Mazzini, A., Svensen, H., Planke, S., Guliyev, I., Akhmanov, G. G., Fallik, T., et al. (2009). When Mud Volcanoes Sleep: Insight from Seep Geochemistry at the Dashgil Mud Volcano, Azerbaijan. *Mar. Pet. Geol.* 26, 1704–1715. doi:10.1016/j.marpetgeo.2008.11.003

Mazzini, A., Scholz, F., Svensen, H. H., Hensen, C., and Hadi, S. (2018). The Geochemistry and Origin of the Hydrothermal Water Erupted at Lusi, Indonesia. *Mar. Pet. Geol.* 90, 52–66. doi:10.1016/j.marpetgeo.2017.06.018

Menzies, M., and Seyfried, W. E. (1979). Basalt-seawater Interaction: Trace Element and Strontium Isotopic Variations in Experimentally Altered Glassy basalt. *Earth Planet. Sci. Lett.* 44, 463–472. doi:10.1016/0012-821X(79)90084-0

Milkov, A. V. (2000). Worldwide Distribution of Submarine Mud Volcanoes and Associated Gas Hydrates. *Mar. Geology*. 167, 29–42. doi:10.1016/S0025-3227(00)00022-0

Millero, F. J., Feistel, R., Wright, D. G., and McDougall, T. J. (2008). The Composition of Standard Seawater and the Definition of the Reference-Composition Salinity Scale. *Deep Sea Res. Oceanogr. Res. Pap.* 55, 50–72. doi:10.1016/j.dsr.2007.10.001

Nauhaus, K., Treude, T., Boetius, A., and Kruger, M. (2005). Environmental Regulation of the Anaerobic Oxidation of Methane: a Comparison of ANME-I and ANME-II Communities. *Environ. Microbiol.* 7, 98–106. doi:10.1111/j.1462-2920.2004.00669.x

Nayak, K., Lin, A. T.-S., Huang, K.-F., Liu, Z., Babonneau, N., Ratzov, G., et al. (2021). Clay-mineral Distribution in Recent Deep-Sea Sediments Around Taiwan: Implications for Sediment Dispersal Processes. *Tectonophysics* 814, 228974. doi:10.1016/j.tecto.2021.228974

Nicholson, K. (1993). *Geothermal Fluids – Chemistry and Exploration Techniques*. London: Springer-Verlag. ISBN-13: 978-3-642-77846-9, e-ISBN-13 :978-3-642-77844-5. 268. doi:10.1007/978-3-642-77844-5

Ohno, T., Komiya, T., Ueno, Y., Hirata, T., and Maruyama, S. (2008). Determination of 88Sr/86Sr Mass-dependent Isotopic Fractionation and Radiogenic Isotope Variation of 87Sr/86Sr in the Neoproterozoic Doushantuo Formation. *Gondwana Res.* 14, 126–133. doi:10.1016/j.gr.2007.10.007

Omrani, H., and Raghimi, M. (2018). Origin of the Mud Volcanoes in the South East Caspian Basin, Iran. *Mar. Pet. Geology.* 96, 615–626. doi:10.1016/j.marpetgeo.2018.05.017

Palmer, M. R., and Edmond, J. M. (1992). Controls over the Strontium Isotope Composition of River Water. *Geochim. Cosmochim. Acta* 56, 2099–2111. doi:10.1016/0016-7037(92)90332-D

Paytan, A., Griffith, E. M., Eisenhauer, A., Hain, M. P., Wallmann, K., and Ridgwell, A. (2021). A 35-Million-Year Record of Seawater Stable Sr Isotopes Reveals a Fluctuating Global Carbon Cycle. *Science* 371, 1346–1350. doi:10.1126/science.aaz9266

Peng, T.-R., Wang, C.-H., Huang, C.-C., Fei, L.-Y., Chen, C.-T. A., and Hwong, J.-L. (2010). Stable Isotopic Characteristic of Taiwan's Precipitation: A Case Study of Western Pacific Monsoon Region. *Earth Planet. Sci. Lett.* 289, 357–366. doi:10.1016/j.epsl.2009.11.024

Perry, E. A., Gieskes, J. M., and Lawrence, J. R. (1976). Mg, Ca and Exchange in the Sediment-Pore Water System, Hole 149, DSDP. *Geochim. et Cosmochim. Acta* 40, 413–423. doi:10.1016/0016-7037(76)90006-5

Planke, S., Svensen, H., HovlandBanks, M. D. A., Banks, D. A., and Jamtveit, B. (2003). Mud and Fluid Migration in Active Mud Volcanoes in Azerbaijan. *Geo-Marine Lett.* 23, 258–268. doi:10.1007/s00367-003-0152-z

Procesi, M., Ciotoli, G., Mazzini, A., and Etiope, G. (2019). Sediment-hosted Geothermal Systems: Review and First Global Mapping. *Earth-Sci. Rev.* 192, 529–544. doi:10.1016/j.earscirev.2019.03.020

Ray, J. S., Kumar, A., Sudheer, A. K., Deshpande, R. D., Rao, D. K., Patil, D. J., et al. (2013). Origin of Gases and Water in Mud Volcanoes of Andaman Accretionary Prism: Implications for Fluid Migration in Forearcs. *Chem. Geology.* 347, 102–113. doi:10.1016/j.chemgeo.2013.03.015

Sano, Y., Kinoshita, N., Kagoshima, T., Takahata, N., Sakata, S., Toki, T., et al. (2017). Origin of Methane-Rich Natural Gas at the West Pacific Convergent Plate Boundary. *Sci. Rep.* 7, 15646. doi:10.1038/s41598-017-15959-5

Scher, H. D., Griffith, E. M., and Buckley, W. P., Jr (2014). Accuracy and Precision of88Sr/86Sr and87Sr/86Sr Measurements by MC-ICPMS Compromised by High Barium Concentrations. *Geochem. Geophys. Geosyst.* 15, 499–508. doi:10.1002/2013GC005134

Seyfried, W. E., and Bischoff, J. L. (1979). Low Temperature basalt Alteration by Sea Water: an Experimental Study at 70°C and 150°C. *Geochimica et Cosmochimica Acta* 43, 1937–1947. doi:10.1016/0016-7037(79)90006-1

Shakirov, R., Obzhirov, A., Suess, E., Salyuk, A., and Biebow, N. (2004). Mud Volcanoes and Gas Vents in the Okhotsk Sea Area. *Geo-mar. Lett.* 24, 140–149. doi:10.1007/s00367-004-0177-y

Shao, Y., Farkaš, J., Mosley, L., Tyler, J., Wong, H., Chamberlayne, B., et al. (2021). Impact of Salinity and Carbonate Saturation on Stable Sr Isotopes (δ88/86Sr) in a Lagoon-Estuarine System. *Geochim. Cosmochim. Acta* 293, 461–476. doi:10.1016/j.gca.2020.11.014

Shih, T. T. (1967). A Survey of the Active Mud Volcanoes in Taiwan and a Study of Their Types and Character of the Mud. *Petrol. Geol. Taiwan* 5, 259–310.

Sun, C.-H., Chang, S.-C., Kuo, C.-L., Wu, J.-C., Shao, P.-H., and Oung, J.-N. (2010). Origins of Taiwan's Mud Volcanoes: Evidence from Geochemistry. *J. Asian Earth Sci.* 37, 105–116. doi:10.1016/j.jseaes.2009.02.007

Teng, L. S. (1990). Geotectonic Evolution of Late Cenozoic Arc-Continent Collision in Taiwan. *Tectonophysics* 183, 57–76. doi:10.1016/0040-1951(90)90188-E

Verma, S. P., and Santoyo, E. (1997). New Improved Equations for , and SiO2 Geothermometers by Outlier Detection and Rejection. *J. Volcanol. Geotherm. Res.* 79, 9–23. doi:10.1016/S0377-0273(97)00024-3

Verma, S. P., Pandarinath, K., and Santoyo, E. (2008). SolGeo: A New Computer Program for Solute Geothermometers and its Application to Mexican Geothermal fields. *Geothermics* 37, 597–621. doi:10.1016/j.geothermics.2008.07.004

Voigt, J., Hathorne, E. C., Frank, M., Vollstaedt, H., and Eisenhauer, A. (2015). Variability of Carbonate Diagenesis in Equatorial Pacific Sediments Deduced from Radiogenic and Stable Sr Isotopes. *Geochim. Cosmochim. Acta* 148, 360–377. doi:10.1016/j.gca.2014.10.001

Voigt, M., Pearce, C. R., Baldermann, A., and Oelkers, E. H. (2018). Stable and Radiogenic Strontium Isotope Fractionation during Hydrothermal Seawater-basalt Interaction. *Geochim. Cosmochim. Acta* 240, 131–151. doi:10.1016/j.gca.2018.08.018

Wei, G., Ma, J., Liu, Y., Xie, L., Lu, W., Deng, W., et al. (2013). Seasonal Changes in the Radiogenic and Stable Strontium Isotopic Composition of Xijiang River Water: Implications for Chemical Weathering. *Chem. Geology.* 343, 67–75. doi:10.1016/j.chemgeo.2013.02.004

Williams, L. B., and Hervig, R. L. (2005). Lithium and boron Isotopes in Illite-Smectite: The Importance of crystal Size. *Geochim. Cosmochim. Acta* 69, 5705–5716. doi:10.1016/j.gca.2005.08.005

Wu, S.-K., Chi, W.-C., Hsu, S.-M., Ke, C.-C., and Wang, Y. (2013). Shallow Crustal Thermal Structures of Central Taiwan Foothills Region. *Terr. Atmos. Ocean. Sci.* 24, 695–707. doi:10.3319/tao.2013.03.13.01(t)

Yang, T. F., Chen, C.-H., Tien, R. L., Song, S. R., and Liu, T. K. (2003). Remnant Magmatic Activity in the Coastal Range of East Taiwan after Arc-Continent Collision: Fission-Track Data and Ratio Evidence. *Radiat. Measurements* 36, 343–349. doi:10.1016/S1350-4487(03)00149-5

Yang, T. F., Yeh, G.-H., Fu, C.-C., Wang, C.-C., Lan, T.-F., Lee, H.-F., et al. (2004). Composition and Exhalation Flux of Gases from Mud Volcanoes in Taiwan. *Env Geol.* 46, 1003–1011. doi:10.1007/s00254-004-1086-0

Yeh, G. H., Yang, T. F., Chen, J. C., Chen, Y. G., and Song, S. R. (2005). "Fluid Geochemistry of Mud Volcanoes in Taiwan," in *Mud Volcanoes, Geodynamics and Seismicity* (Dordrecht: Springer), 227–237.

Yoshimura, T., Wakaki, S., Ishikawa, T., Gamo, T., Araoka, D., Ohkouchi, N., et al. (2020). A Systematic Assessment of Stable Sr Isotopic Compositions of Vent Fluids in Arc/back-Arc Hydrothermal Systems: Effects of Host Rock Type, Phase Separation, and Overlying Sediment. *Front. Earth Sci.* 8, 591711. doi:10.3389/feart.2020.591711

You, C.-F., Gieskes, J. M., Lee, T., Yui, T.-F., and Chen, H.-W. (2004). Geochemistry of Mud Volcano Fluids in the Taiwan Accretionary Prism. *Appl. Geochem.* 19, 695–707. doi:10.1016/j.apgeochem.2003.10.004

Yu, S.-B., Chen, H.-Y., and Kuo, L.-C. (1997). Velocity Field of GPS Stations in the Taiwan Area. *Tectonophysics* 274, 41–59. doi:10.1016/S0040-1951(96)00297-1

Zachos, J. C., Dickens, G. R., and Zeebe, R. E. (2008). An Early Cenozoic Perspective on Greenhouse Warming and Carbon-Cycle Dynamics. *Nature* 451, 279–283. doi:10.1038/nature06588

Conflict of Interest: In-Tian Lin is employed by the Exploration and Development Research Institute, CPC Corporation.

The remaining authors declare that the research was conducted in the absence of any commercial or financial relationships that could be construed as a potential conflict of interest.

Publisher's Note: All claims expressed in this article are solely those of the authors and do not necessarily represent those of their affiliated organizations, or those of the publisher, the editors, and the reviewers. Any product that may be evaluated in this article, or claim that may be made by its manufacturer, is not guaranteed or endorsed by the publisher.